# APPROXIMATION OF UNKNOWN SOURCES IN A TIME FRACTIONAL PDE BY THE OPTIMAL ONES AND THEIR RECONSTRUCTION

MOURAD HRIZI, RAVI PRAKASH, AND ANTONIO ANDRÉ NOVOTNY

Abstract. In this paper, our focus is on studying a geometric inverse source problem that is governed by two-dimensional time-fractional subdiffusion. The problem involves determining the shape and location of the unknown source's geometrical support from boundary measurements of its associated potential. Firstly, we prove the uniqueness of the inverse problem. In the second phase, we propose a novel reconstruction method that utilizes the coupled complex boundary method (CCBM) to solve the identification problem. The main idea of this method is to approximate the overdetermined problem to a complex boundary value problem with a complex Robin boundary condition coupling the Dirichlet and Neumann boundary conditions. Next, we utilize the imaginary part of the solution throughout the domain to construct a shape cost function, which we then minimize with respect to ball-shaped sources by using a Newton-type topological derivative method to reconstruct the geometrical support of the unknown source.

## 1. Introduction

Time-fractional subdiffusion equation is a powerful tool to model the dynamics of physical processes that exhibit anomalously slow diffusion. This modeling technique has found successful applications in a range of fields, including contaminant transport in underground water [11], kinetic and reaction-diffusion processes [18, 72], plasma physics [14], neuronal modeling in biology [23], and the study of viscoelasticity dynamics [29]. In such processes, several model parameters cannot be directly measured or specified, and must be inferred indirectly from available data [19, 58, 78, 77]. This leads to a range of inverse problems. For a comprehensive overview, we refer to [45].

This article analyzes an inverse source problem associated with a two-dimensional time-fractional diffusion equation of order $0 < \alpha < 1$, also known as subdiffusion equation. For the mathematical formulation, let us consider an open and bounded domain $\Omega$ in $\mathbb{R}^2$ with a sufficiently smooth boundary $\partial\Omega$. Furthermore, for a fixed terminal time $T > 0$, we consider the diffusion process in $\Omega$ which is governed by the boundary value problem

$$\left\{\begin{array}{rcll} \partial_t^\alpha \boldsymbol{u} - \Delta \boldsymbol{u} + \boldsymbol{u} &=& F^* & \text{in} \quad (0,T)\times\Omega, \\ \boldsymbol{u} &=& \varphi & \text{on} \quad (0,T)\times\partial\Omega, \\ \boldsymbol{u}(.,0) &=& 0 & \text{in} \quad \Omega. \end{array}\right. \tag{1}$$

In this model, $\boldsymbol{u}$ represents the concentration for the diffusion process, $\varphi$ is a given Dirichlet data, and $F^*$ is the (unknown) source term. The notation $\partial_t^\alpha$ denotes the Caputo fractional left derivative of order $0 < \alpha < 1$ with respect to $t$. It is defined as (see, e.g., [51, p.91])

$$\partial_t^\alpha \boldsymbol{u}(t,x) := \frac{1}{\Gamma(1-\alpha)} \int_0^t (t-\tau)^{-\alpha} \frac{\partial \boldsymbol{u}}{\partial \tau}(\tau,x)\mathrm{d}\tau, \quad (t,\, x) \in (0,\, T)\times\Omega.$$

Here, $\Gamma$ denotes Euler's Gamma function, which is defined, for $z \in \{z \in \mathbb{C} : \Re\{z\} > 0\}$, as

$$\Gamma(z) = \int_0^\infty s^{z-1} e^{-s} \mathrm{d}s.$$

It is known that as $\alpha \longrightarrow 1^-$, the Caputo fractional derivative $\partial_t^\alpha \boldsymbol{u}$ converges to the usual first-order derivative $\partial_t \boldsymbol{u}$ (see, e.g., [34, p. 68]), and as a result, the model (1) simplifies to the

*Key words and phrases.* Inverse source problem, time-fractional subdiffusion, coupled complex boundary method, topological derivative method.

classical diffusion equation. According to [2], model (1) belongs to the class of time-fractional diffusion equations, which are effective for modeling anomalous diffusion phenomena in heterogeneous media. At the microscopic level, the model can be explained by a continuous time random walk, where the waiting time distribution between consecutive jumps is heavy-tailed with a divergent mean. This behavior is analogous to Brownian motion in the standard diffusion equation (See [68]). We refer interested readers to the comprehensive reviews [63, 62] for other physical motivations of the mathematical model and long lists of successful applications. These practical applications have drawn significant attention from mathematical researchers in recent years, and consequently, equation (1) has become an important model for active mathematical research community. In [79], Yamamoto analyses the existence of unique weak solutions and establishes an apriori estimates for the time-fractional diffusion problem (1) with $F^* = 0$ and non-zero Dirichlet boundary data $\varphi$, which belong to the finite energy space $L^2$ in time $t$ and to a Sobolev space of negative order in space. In contrast, Kemppainen and Ruotsalainen have studied this problem for $\varphi$ belonging to Sobolev spaces of positive order in space (See [47]). Gorenflo, Luchko, and Yamamoto, in [32], have redefined the Caputo derivative in fractional Sobolev spaces and studied (1) from an operator theory perspective. Meanwhile, Sakamoto and Yamamoto have analyzed the well-posedness and asymptotic behavior of the solution to (1) in [69]. More recently, Kian and Yamamoto, in [50], has studied the well-posedness of problem (1) in both strong and weak senses. For numerical treatments, we refer to [43, 44] for the finite element method and [57, 60] for the finite difference method.

In this article, our goal is to solve the inverse problem of recovering the source term $F^*$ of the governing equation (1) using boundary measurements. However, it is widely recognized that boundary measurements alone are typically insufficient to uniquely determine a general source $F^*$ (as discussed, for instance, in [48]), and additional assumptions must be imposed to enable unique recovery. To address this issue, we assume that the source term $F^*$ can be decomposed into contributions from space and time variables. Specifically, we aim to determine an unknown source of the form

$$F^*(t,x) = \zeta(t)\, f^*(x) \quad \text{for all } (t,\, x) \in (0,\, T) \times \Omega.$$

In this context, $f^*$ represents the magnitude of the source term that depends on the spatial variable, while $\zeta$ denotes the attenuation factor that accounts for the time dependence of the diffusion phenomenon.

In recent years, there has been a surge of theoretical and numerical approaches aimed at identifying $F^*(t,x) = \zeta(t)f^*(x)$, driven by the importance of this equation in both scientific and industrial contexts. These approaches can be classified into two main groups:

(i) Inverse $t$-source problem of recovering $\zeta$: This case involves identifying the temporal component $\zeta$ of the source term $F^*$. The assumption is that the spatial component $f^*$ is already known. This problem has been extensively studied in the literature, and several methods have been proposed to address it. See [27, 55, 69, 76].

(ii) Inverse $x$-source problem of recovering $f^*$ : Here, the goal is to identify the spatial component $f^*$ of the source term $F^*$, assuming that the temporal component $\zeta$ is known. This problem has been studied in various contexts, and several techniques have been proposed to address it. Relevant literature includes [70, 81, 39, 41, 78, 77, 75]. Note that all previous works focused on recovering either $\zeta(t)$ or $f^*(x)$ individually. However, [48] demonstrated the simultaneous recovery of both functions under appropriate assumptions. For more information on the theoretical and numerical results, interested readers may consult the reviews [45, 59]. In addition, it is worth mentioning the recent works [42, 49] that focus on the reconstruction of a source term of the form $F^*(t,x) = \zeta(t,x)f^*(t,x')$, where $x \in \mathbb{R}^d$ and $x' \in \mathbb{R}^{d-1}$, $d \geq 2$, $f^*$ is unknown, and $\zeta$ is a given function of $t$ and $x$ both.

In the classical parabolic setting (i.e., $\alpha = 1$), inverse source problems of this kind are directly relevant to several real-world applications. A prominent example is the transport

of contaminants in groundwater, where the task is to reconstruct the origin and timing of a pollutant release based on concentration data collected at observation wells or along the domain boundary [10, 25]. Similar inverse problems also arise in biomedical engineering, notably in the identification of internal heat sources in thermal-wave models of bio-heat transfer [4], as well as in the reconstruction of source distributions in bioluminescence tomography [74].

This paper aims to solve the same inverse problem as in [36, 65, 68], which involves reconstructing the geometrical support of an unknown, space-dependent source term, $f^*$, using boundary measurements of the associated potential. To conclude, we briefly outline the structure of the paper. Section 2 is about describing the inverse problem under consideration and provide the relevant existing results. In Section 3, we prove an identifiability result for the inverse source problem using Duhamel's principle whereas, in Section 4, we introduce a new coupled complex boundary method suitable for our problem and its reformulation as shape optimization problem by including a least-squares fitting for the imaginary part of the complex time-fractional diffusion solution. Section 4.1 describes the existence and uniqueness of a weak solution for the direct complex time-fractional diffusion problem. In Section 4.2, we investigate the continuous dependence of the solution (of a complex valued problem) on its source term. Section 5 provides theoretical results on the existence and stability of the shape optimization problem. We prove the convergence of optimal shape to the solution of inverse problem at hand in Section 6. Section 7 analyzes the crucial regularization issue and derives a second-order topological asymptotic expansion of a least-square functional with respect to a finite number of circular holes. Finally, a set of numerical examples are presented in Section 8, showing varying features of the proposed non-iterative reconstruction algorithm, including its robusteness with respect to noisy data. The paper ends with some concluding remarks through Section 9.

## 2. Problem Formulation

For a given non-null function $\zeta$ in $L^2(0,\,T)$, let us consider the problem

$$\left\{\begin{array}{rcll} \partial_t^\alpha \boldsymbol{u} - \Delta \boldsymbol{u} + \boldsymbol{u} &=& \zeta(t)\chi_{\mathcal{D}^*} & \text{in} \quad (0,T)\times\Omega, \\ \boldsymbol{u} &=& \varphi & \text{on} \quad (0,T)\times\partial\Omega, \\ \boldsymbol{u}(.,0) &=& 0 & \text{in} \quad \Omega, \end{array}\right. \tag{2}$$

where $\chi_{\mathcal{D}^*}$ is the characteristic function of the *unknown* subdomain $\mathcal{D}^* \subset \Omega$. The inverse problem under investigation is to reconstruct the location and shape of the spatial component $f^* = \chi_{\mathcal{D}^*}$ from the additional inversion input data

$$\phi(t,\,x) = \partial_\nu \boldsymbol{u}(t,\,x), \quad (t,\,x) \in (0,\,T)\times\partial\Omega, \tag{3}$$

where $\nu$ is the outward unit normal vector to $\partial\Omega$ and $\partial_\nu \boldsymbol{u} = \nabla \boldsymbol{u}.\nu$.

Rundell and Zhang, in [68], introduced a Newton-type iterative method for reconstructing the shape of the characteristic function $f^* = \chi_{\mathcal{D}^*}$. To tackle the ill-posed nature of the problem, they combined a prior assumption on $\mathcal{D}^*$ with Tikhonov's method, resulting in the Levenberg-Marquardt-type formula. This approach deals with the reconstruction of shape of characteristic function even with limited data or noisy measurements. In [36], the current inverse source problem is reformulated as an optimization problem using Tikhonov regularization, which can be expressed as follows :

$$\underset{\mathcal{D}\subset\Omega}{\text{Minimize}}\; j(\mathcal{D}) := \frac{1}{2}\int_0^T \int_{\partial\Omega} \left|\partial_\nu \boldsymbol{u} - \phi\right|^2 \mathrm{d}s\mathrm{d}t + \eta_1\, P_\Omega(\mathcal{D}), \tag{4}$$

where $\boldsymbol{u}$ is a weak solution of the boundary value problem (1) with $F^* = \chi_{\mathcal{D}}$, $\eta_1 > 0$ represents the regularization parameter and $P_\Omega(\mathcal{D})$ denotes the relative perimeter of the subdomain $\mathcal{D}$ in

$\Omega$ which is defined according to the De Giorgi formula

$$P_\Omega(\mathcal{D}) = \sup\Big\{ \int_{\mathcal{D}} \operatorname{div}(\vartheta(x))\,\mathrm{d}x \,\Big|\, \vartheta : \Omega \longrightarrow \mathbb{R}^2, \\ \vartheta \ \text{ is smooth with } \operatorname{supp}(\vartheta) \subset \Omega \text{ and } \|\vartheta(x)\|_\infty \leq 1 \ \forall x \in \Omega\Big\},$$

where $\|\cdot\|_\infty$ is the essential supremum norm. In that paper, Hu and Zhu put forward a level set method that utilizes shape sensitivity analysis for reconstructing the shape of $\mathcal{D}^*$. On the other hand, in [65], a Kohn-Vogelius type cost function is used for data fitting. In general, Kohn–Vogelius functionals are expected to lead to more robust optimization procedures. In this case, one has to find a stable approximate spatial source function $f^* = \chi_{\mathcal{D}^*}$ through the following optimization problem:

$$\underset{\chi_{\mathcal{D}} \in Q_{ad}}{\text{Minimize}}\, \mathcal{J}(\chi_{\mathcal{D}}) := \int_0^T \int_\Omega \Big|\nabla\Big(u_D - u_N\Big)\Big|^2 \mathrm{d}x\mathrm{d}t + \eta_2 P_\Omega(\mathcal{D}), \tag{5}$$

where $\eta_2$ is a regularization parameter, $Q_{ad}$ is an admissible set of characteristic functions. Moreover, $u_D$ and $u_N$ are the weak solutions of the boundary value problems

$$\begin{cases} \partial_t^\alpha u_D - \Delta u_D + u_D &= \zeta\,\chi_{\mathcal{D}} \quad \text{in} \quad (0,\,T)\times\Omega, \\ u_D &= \varphi \quad \text{on} \quad (0,\,T)\times\partial\Omega, \\ u_D(.,0) &= 0 \quad \text{in} \quad \Omega, \end{cases} \tag{6}$$

and

$$\begin{cases} \partial_t^\alpha u_N - \Delta u_N + u_N &= \zeta\,\chi_{\mathcal{D}} \quad \text{in} \quad (0,\,T)\times\Omega, \\ \partial_\nu u_N &= \phi \quad \text{on} \quad (0,\,T)\times\partial\Omega, \\ u_N(.,0) &= 0 \quad \text{in} \quad \Omega, \end{cases} \tag{7}$$

respectively. Hence, it is clear that both optimization problems, namely (4) and (5), use Neumann data $\phi$ and Dirichlet data $\varphi$ in a sequential manner. However, as a novelty of this paper, we propose a different approach, called as coupled complex boundary method (CCBM), which utilizes both data in a single boundary value problem. The key idea behind this method is to couple the Neumann and Dirichlet data using a Robin boundary condition, where the Neumann data and Dirichlet data correspond to the real and imaginary parts of the Robin boundary condition, respectively. The CCBM method, initially proposed by Cheng, Gong, Han, and Zheng in [20]. It aims to recover the source term $p \in L^2(\Omega)$ in the elliptic equation $-\Delta u + u = p\chi_{\mathcal{D}}$, given that the source support $\mathcal{D}$ is known. CCBM has been extended to various inverse problems. For instance, it has been applied to inverse conductivity reconstruction from a single boundary measurement [31], and to parameter identification in elliptic problems [82]. In [66], the method was further adapted to a shape optimization framework for numerically solving the exterior Bernoulli free boundary problem. More recently, CCBM has also been employed in inverse obstacle problems [3, 67]. To the best of our knowledge, this work represents the first application of the coupled complex boundary condition concept to a fractional inverse problem. With the help of CCBM method, we reformulate the considered inverse problem which deals in finding the unknown space-dependent source that causes the imaginary part of the solution of a new complex boundary value problem to vanish within the domain $\Omega$. To achieve this, the problem is reformulated as a topology optimization one where the source distribution is the unknown variable. To be more precise, the topology optimization consists in minimizing a least-square functional enhanced with a regularization term which penalizes the perimeter of the unknown support of the space-dependent source term. Some theoretical analysis results have been discussed. Specifically, we establish the existence of the regularized optimization problem, investigate the stability of this problem under small perturbations of the measured data, and demonstrate the convergence of a subsequence of optimal solutions to the solution of the inverse problem when the noise level (of the observation data $\phi$) goes to zero. In practice, the numerical solution of the regularized optimization problem can be

challenging due to the non-differentiability of the cost function that needs to be minimized, which arises from the regularization term. To address this issue, we propose a self-regularized method using topological sensitivity analysis which is introduced in the book [64]. For the reconstruction of location, shape, and number of source distributions within the geometrical domain $\Omega$, we utilize an asymptotic expansion of the least-squares functional with respect to a finite number of ball-shaped trial sources. We developed an efficient and fast one-shot reconstruction algorithm using second-order topological sensitivity. Notably, in this paper, we present a novel computational algorithmic approach that addresses current challenges in the field and yields significantly improved numerical results compared to those reported in [65].

The CCBM method offers an advantage over classical methods by enabling the definition of the cost function (to be minimized) throughout the entire domain $\Omega$. This leads to a more robust reconstruction compared to least-squares type functions, which are limited to the boundary. While it may be challenging to demonstrate the superiority of the proposed complex coupled formulation over the Kohn-Vogeluis method from a theoretical standpoint, the numerical examples provided in this paper suggest that it produces equivalent reliable results for the inverse problem at hand, but with half computational effort.

## 3. Uniqueness of inverse Source problem

In this section, we demonstrate that the spatial source term $f^* = \chi_{\mathcal{D}^*}$ of (2) can be uniquely determined from the boundary measurement $\phi$ of the potential field $\boldsymbol{u}$ on $\partial\Omega$. Recall that Rundell and Zhang, in [68], established the uniqueness of determining the subdomain $\mathcal{D}^*$ (when $\zeta = 1$) from measurements of the solution at a finite number of points on the boundary $\partial\Omega$, where $\mathcal{D}^*$ is an unknown star-like subdomain and $\Omega$ being a unit disc. In [65], authors also showed that the space-dependent source term $f^* = \chi_{\mathcal{D}^*}$ can be uniquely determined from boundary measurement data, provided that $\zeta \in C^1([0,T])$ with $\zeta(0) \neq 0$. In the current article, we address the issue of uniqueness of the considered inverse problem when the time-dependent function $\zeta$ belongs to the functional space $L^2(0,T)$ without having an additional assumption $\zeta(0) \neq 0$. In other words, one of the novelty of this paper is to establish the existing results for a less regular data. To this end, we introduce relevant function spaces and auxiliary results.

For $1 \leq p < \infty$, let $L^p(\Omega)$, $H_0^1(\Omega)$, $H^1(\Omega)$ and $H^2(\Omega)$ be the usual classical real Lebesgue and Sobolev spaces. We define the fractional Sobolev-Slobodecki space $H^\alpha(0,T)$ on the interval $(0,T)$ with the norm in $H^\alpha(0,T)$

$$\Big\|\kappa\Big\|_{H^\alpha(0,T)} = \Big(\Big\|\kappa\Big\|^2_{L^2(0,T)} + \int_0^T\int_0^T \frac{|\kappa(t)-\kappa(\tau)|^2}{|t-\tau|^{1+2\alpha}}\,\mathrm{d}t\mathrm{d}\tau\Big)^{1/2}$$

for $0 < \alpha < 1$ and set

$${}_0H^\alpha(0,T) = \Big\{\kappa \in H^\alpha(0,T):\ \kappa(0) = 0\Big\} \quad \text{if } 1/2 < \alpha < 1.$$

Moreover, we define the Banach spaces $H_\alpha(0,T)$ as (see, e.g., Kubica, Ryszewska and Yamamoto [52])

$$H_\alpha(0,T) = \begin{cases} H^\alpha(0,T), & \text{if } 0 < \alpha < 1/2,\\ \Big\{\kappa \in H^{1/2}(0,T):\ \displaystyle\int_0^T \frac{|\kappa(t)|^2}{t}\mathrm{d}t < \infty\Big\}, & \text{if } \alpha = 1/2,\\ {}_0H^\alpha(0,T), & \text{if } 1/2 < \alpha < 1. \end{cases}$$

The norm in $H_\alpha(0,T)$ is equivalent to

$$\Big\|\kappa\Big\|_{H_\alpha(0,T)} = \begin{cases} \Big\|\kappa\Big\|_{H^\alpha(0,T)}, & 0 < \alpha < 1,\ \ \alpha \neq 1/2,\\ \Big(\Big\|\kappa\Big\|^2_{H^{1/2}(0,T)} + \displaystyle\int_0^T \frac{|\kappa(t)|^2}{t}\mathrm{d}t\Big)^{1/2}, & \alpha = 1/2. \end{cases}$$

Define the forward Riemann-Liouville integral operator as

$$\Big(J_\alpha \kappa\Big)(t) = \frac{1}{\Gamma(\alpha)} \int_0^t (t-\tau)^{\alpha-1} \kappa(\tau)\, \mathrm{d}\tau, \quad 0 < t < T, \quad \kappa \in D(J_\alpha) = L^2(0,\, T), \tag{8}$$

where $D(J_\alpha)$ denotes the domain of the operator $J_\alpha$. Regarding the operator $J_\alpha$ and the space $H_\alpha(0,\, T)$, we have the following lemmas:

**Lemma 1.** *(see* [52, Lemma 1.3(iv)]*). For $\alpha_1, \alpha_2 > 0$, we have*

$$J_{\alpha_1+\alpha_2} = J_{\alpha_1} J_{\alpha_2} = J_{\alpha_2} J_{\alpha_1} \quad \textit{in} \quad L^2(0,\, T).$$

**Lemma 2.** *If $0 < \alpha < 1$, then*

$$J_\alpha :\ L^2(0,\, T) \longrightarrow H_\alpha(0,\, T) \quad \textit{is bijective and isomorphism.} \tag{9}$$

For the proof of Lemma 2, see Kubica, Ryszewska and Yamamoto [52, Theorem 2.1], Yamamoto [80], Gorenflo, Luchko and Yamamoto [32]. Since $J_\alpha$ is bijective in $L^2(0,\, T)$, $(J_\alpha)^{-1}$ exists and by $J_{-\alpha} = (J_\alpha)^{-1}$, we denote the algebraic inverse to $J_\alpha$. Hence, we can redefine the Caputo derivative $\partial_t^\alpha$ for functions in $H_\alpha(0,\, T)$.

**Definition 3.** *(see* [52, Definition 2.1]*). For $0 \le \alpha \le 1$, we recall that*

$$\partial_t^\alpha \kappa := J_{-\alpha} \kappa = (J_\alpha)^{-1} \kappa, \quad \kappa \in H_\alpha(0,\, T) \tag{10}$$

*with the domain $D(\partial_t^\alpha) = H_\alpha(0,\, T)$. We recall that, $D(\partial_t^\alpha)$ denotes the domain of the operator $\partial_t^\alpha$.*

We now demonstrate a key property of $\partial_t^\alpha$ for the convolution of two functions, when $D(\partial_t^\alpha) = H_\alpha(0, T)$. To present this property, we denote

$$\psi * \theta(t) = \int_0^t \psi(t-\tau)\theta(\tau)\mathrm{d}\tau, \quad 0 < t < T \tag{11}$$

for $\psi \in L^2(0,\, T)$ and $\theta \in L^1(0,\, T)$. Then the Young inequality on the convolution yields

$$\Big\| \psi * \theta \Big\|_{L^2(0,T)} \le \Big\| \psi \Big\|_{L^2(0,T)} \Big\| \theta \Big\|_{L^1(0,T)}. \tag{12}$$

Now, we recall an important result which plays a vital role in establishing relation between convolution and fractional derivative.

**Lemma 4.** *(see* [80, Theorem 4]*). Let $\alpha \ge 0$. Then for $\psi \in H_\alpha(0,\, T)$ and $\theta \in L^1(0,\, T)$, we have $\psi * \theta \in H_\alpha(0,\, T)$ and*

$$\partial_t^\alpha \big(\psi * \theta\big) = \partial_t^\alpha \big(\psi\big) * \theta.$$

In the next lemma, we present a well-known theorem in the theory of complex analysis, namely, Titchmarsh convolution theorem. The proof of this lemma can be found in [73, Theorem VII] (see also [46]).

**Lemma 5.** *(Titchmarsh's theorem). If $\psi(t)$ and $\theta(t)$ are integrable functions, such that*

$$\psi * \theta(t) = \int_0^t \psi(\tau)\theta(t-\tau)\mathrm{d}\tau = 0, \quad 0 < t < T,$$

*then $\psi(t) = 0$ almost everywhere in $(0, T_1)$ and $\theta(t) = 0$ almost everywhere in $(0, T_2)$, where $T_1 + T_2 \ge T$.*

Next, we establish Duhamel's principle in $H_\alpha(0,\, T)$-space for time-fractional parabolic equations.

3.1. **Duhamel's principle.** For $0 < \alpha < 1$, $\gamma \in L^2(0,T)$ and $g \in L^2(\Omega)$, we consider the following time-fractional diffusion problem

$$\partial_t^\alpha w - \Delta w + w = \gamma\, g \ \text{ in } \ L^2(0,T;L^2(\Omega)), \tag{13}$$

$$w \in H_\alpha(0,T;L^2(\Omega)) \cap L^2(0,T;H^2(\Omega)\cap H_0^1(\Omega)). \tag{14}$$

Based on the findings of Kubica, Ryszewska, and Yamamoto [52], the problem (13)-(14) has a unique solution. Now, we prove the following lemma :

**Lemma 6.** *For $0 < \alpha < 1$, let $\vartheta := J_{1-\alpha} w$ with $w$ being the unique solution of* (13)-(14)*. Then $\vartheta$ satisfies*

$$\begin{cases} \partial_t^\alpha \vartheta - \Delta\vartheta + \vartheta = (J_{1-\alpha}\gamma)\, g \ \text{ in } \ L^2(0,T;L^2(\Omega)), \\ \vartheta \in H_\alpha(0,T;L^2(\Omega)) \cap L^2(0,T;H^2(\Omega)\cap H_0^1(\Omega)). \end{cases} \tag{15}$$

*Proof.* By definition, we have

$$\vartheta \in L^2\left(0,T;H^2(\Omega)\cap H_0^1(\Omega)\right). \tag{16}$$

Now, using (8), we can write $\vartheta$ as

$$\vartheta(t,\cdot) = J_{1-\alpha} w(t,\cdot) = \frac{1}{\Gamma(1-\alpha)} \int_0^t (t-\tau)^{-\alpha} w(\tau,\cdot)\mathrm{d}\tau = \theta_\alpha * \psi(t), \quad 0 < t < T,$$

where

$$\theta_\alpha(t) = \frac{t^{-\alpha}}{\Gamma(1-\alpha)} \quad \text{and} \quad \psi(t) = w(t,\cdot).$$

Since $\theta_\alpha \in L^1(0,T)$ and $\psi \in H_\alpha\left(0,T;L^2(\Omega)\right)$, we can apply Lemma 4 to conclude that

$$\vartheta \in H_\alpha\left(0,T;L^2(\Omega)\right). \tag{17}$$

Thus, from (16) and (17), we can conclude that $\vartheta \in H_\alpha\left(0,T;L^2(\Omega)\right) \cap L^2\left(0,T;H^2(\Omega)\cap H_0^1(\Omega)\right)$.

Next, we prove that $\vartheta$ satisfies the first equation in (15). By applying Lemma 2, we know that the operator $J_{1-\alpha}$ is injective on $L^2(0,T)$. Operating $J_{1-\alpha}$ on the left-hand side of equation (13) yields the following expression:

$$J_{1-\alpha}\left(\partial_t^\alpha w\right) - \Delta\left(J_{1-\alpha} w\right) + J_{1-\alpha} w = \left(J_{1-\alpha}\gamma\right) g. \tag{18}$$

By using $w \in H_\alpha(0,T;L^2(\Omega))$ and (10), we have

$$\partial_t^\alpha w = J_{-\alpha} w.$$

Additionally, we can apply Lemma 1 to obtain

$$J_\alpha J_{1-\alpha} = J_1, \tag{19}$$

where $J_1$ is defined by the following integral

$$(J_1 y)(t) = \int_0^t y(\tau)\,\mathrm{d}\tau \quad \text{for } \ 0 \le t \le T. \tag{20}$$

We can apply $(J_\alpha)^{-1}$ to both sides of equation (19), which gives us

$$J_\alpha J_{1-\alpha}\left(J_\alpha\right)^{-1} = J_{1-\alpha}. \tag{21}$$

By applying $(J_\alpha)^{-1}$ to the left-hand side of (21) and using the fact that $(J_\alpha)^{-1} J_\alpha u = u$ for $u$ in $L^2(0,,T)$ [52, Corollary 2.1], we obtain

$$J_{1-\alpha}\left(J_\alpha\right)^{-1} = \left(J_\alpha\right)^{-1} J_{1-\alpha}. \tag{22}$$

This implies that $J_{1-\alpha}\left(\partial_t^\alpha\right) = \partial_t^\alpha\left(J_{1-\alpha}\right)$. Therefore, we can now rewrite the identity (18) as

$$\partial_t^\alpha\left(J_{1-\alpha} w\right) - \Delta\left(J_{1-\alpha} w\right) + J_{1-\alpha} w = \left(J_{1-\alpha}\gamma\right) g.$$

Hence the fact. □

We are now well-prepared to state Duhamel's principle, which transforms the solution to an initial-boundary value problem without source term (i.e. the source term is equal to zero) to a solution of (15).

**Lemma 7.** *(Duhamel's principle in $H_\alpha(0,T)$). Given $\gamma \in L^2(0,,T)$ and $g \in L^2(\Omega)$, let $w$ be the solution of* (13)-(14)*. Then, $J_{1-\alpha}w$ can be represented as*

$$J_{1-\alpha}w(t,x) = \int_0^t \gamma(\tau)v(t-\tau,x)\mathrm{d}\tau, \quad (t,\, x) \in (0,\, T) \times \Omega,$$

*where $v$ satisfies the following system*

$$\begin{cases} \partial_t^\alpha\Big(v-g\Big) - \Delta v + v = 0 \ \ in \ \ L^2(0,T;L^2(\Omega)), \\ \\ v - g \in H_\alpha(0,T;L^2(\Omega)), \\ \\ v \in L^2(0,T;H^2(\Omega)\cap H_0^1(\Omega)). \end{cases} \tag{23}$$

*Proof.* The existence and uniqueness of a weak solution $v \in H_\alpha(0,T;L^2(\Omega)) \cap L^2(0,T;H^2(\Omega)\cap H_0^1(\Omega))$ of (23) can be found in [52]. We define

$$\Psi(t,x) := \int_0^t \gamma(\tau)v(t-\tau,x)\mathrm{d}\tau, \quad (t,\, x) \in (0,\, T) \times \Omega.$$

Firstly, we show that $\Psi \in H_\alpha\left(0,T;L^2(\Omega)\right) \cap L^2(0,T;H^2(\Omega)\cap H_0^1(\Omega))$.
Since $v \in L^2\left(0,T;H^2(\Omega)\cap H_0^1(\Omega)\right)$, by employing the same argument as in the proof of Lemma 6, we can conclude that

$$\Psi \in L^2\left(0,T;H^2(\Omega)\cap H_0^1(\Omega)\right). \tag{24}$$

We now proceed to demonstrate that $\Psi \in H_\alpha\left(0,T;L^2(\Omega)\right)$. We can write $\Psi$ as

$$\Psi(t,x) = \Psi_1(t,x) + \Psi_2(t,x), \quad (t,\, x) \in (0,\, T) \times \Omega,$$

where $\Psi_1$ and $\Psi_2$ are defined respectively by

$$\Psi_1(t,\cdot) := \int_0^t \gamma(\tau)(v-g)(t-\tau,\cdot)\mathrm{d}\tau \quad \text{in } \ \Omega, \quad 0 < t < T,$$

and

$$\Psi_2(t,\cdot) := \left(J_1\gamma\right)(t)g(\cdot) \quad \text{in } \Omega, \ \ 0 < t < T.$$

Here, the integral $t \longmapsto J_1\gamma(t)$ is defined in (20). We will now examine the regularity of the functions $\Psi_1$ and $\Psi_2$.

Note that $\Psi_1(t,\cdot) = \gamma * \psi(t)$, where $\psi(t) = (v-g)(t,\cdot)$. Since $v - g \in H_\alpha\left(0,T;L^2(\Omega)\right)$ and $\gamma \in L^2(0,T)$, we can conclude from Lemma 4 that

$$\Psi_1 \in H_\alpha\left(0,T;L^2(\Omega)\right). \tag{25}$$

Next, we show that $\Psi_2 \in H_\alpha(0,T;L^2(\Omega))$. Using that the operator $J_{-\alpha} : H_\alpha(0,T) \longrightarrow L^2(0,T)$ is surjective and $\gamma \in L^2(0,T)$, there exists $\theta \in H_\alpha(0,T)$ such that

$$\gamma = J_{-\alpha}\theta = (J_\alpha)^{-1}\theta.$$

Hence,

$$J_1\gamma = J_1\left(J_{-\alpha}\theta\right) = J_{1-\alpha}\theta.$$

According to (8), we have

$$J_1\gamma(t) = \frac{1}{\Gamma(1-\alpha)}\int_0^t (t-\tau)^{-\alpha}\theta(\tau)\mathrm{d}\tau := \psi_\alpha * \theta(t),$$

where

$$\psi_\alpha(t) = \frac{t^{-\alpha}}{\Gamma(1-\alpha)}.$$

Since, $\psi_\alpha \in L^1(0,T)$ and $\theta \in H_\alpha(0,T)$, by Lemma 4, we have $J_1\gamma \in H_\alpha(0,T)$. Moreover, since $g \in L^2(\Omega)$, we have

$$\Psi_2 \in H_\alpha\left(0,T;L^2(\Omega)\right). \tag{26}$$

Consequently, from (25) and (26), we get

$$\Psi = \Psi_1 + \Psi_2 \in H_\alpha\left(0,T;L^2(\Omega)\right). \tag{27}$$

Combining (24) and (27), we can conclude that $\Psi \in H_\alpha\left(0,T;L^2(\Omega)\right) \cap L^2(0,T;H^2(\Omega)\cap H_0^1(\Omega))$.

Now, we prove that $\Psi$ satisfies the first equation in (15). By utilizing Lemma 4 and the fact that $\big(v-g\big) \in H_\alpha(0,T;L^2(\Omega))$, we can write

$$\partial_t^\alpha \Psi = \partial_t^\alpha \Psi_1 + \partial_t^\alpha \Psi_2 = \int_0^t \gamma(\tau)\partial_t^\alpha\big(v-g\big)(t-\tau,\cdot)\mathrm{d}\tau + \partial_t^\alpha\left(J_1\gamma\right)(t)g.$$

On the other hand, from Definition 3 and Lemma 1, we can write

$$\partial_t^\alpha\left(J_1\gamma\right)(t) = \left(J_\alpha\right)^{-1}\left(J_1\gamma\right)(t) = J_{1-\alpha}\gamma(t), \quad 0<t<T.$$

Additionally, we have

$$\Delta\Psi = \int_0^t \gamma(\tau)\Delta v(t-\tau,\cdot)\mathrm{d}\tau.$$

Thus,

$$\partial_t^\alpha\Psi - \Delta\Psi + \Psi = \int_0^t \gamma(\tau)\Big[\partial_t^\alpha\big(v-g\big)(t-\tau,\cdot) - \Delta v(t-\tau,\cdot) + v(t-\tau,\cdot)\Big]\mathrm{d}\tau + J_{1-\alpha}\gamma(t)g(\cdot).$$

Since $v$ satisfies (23), it follows that

$$\partial_t^\alpha\Psi - \Delta\Psi + \Psi = \big(J_{1-\alpha}\gamma\big)g.$$

Hence, uniqueness of the solution of (15) (see, for example, [52]) implies $\Psi = J_{1-\alpha}w$. □

**Remark 8.** *We observe that the term $\partial_t^\alpha\big(v-g\big)$ in (23) is well-defined due to the second condition in (23). Specifically, for $\frac{1}{2} < \alpha < 1$, the Sobolev embedding yields the inclusions $H_\alpha(0,T) \subset H^\alpha(0,T) \subset C[0,T]$. Consequently, $(v-g) \in H_\alpha\left(0,T;L^2(\Omega)\right)$ implies $(v-g) \in C\left([0,T];L^2(\Omega)\right)$. In this scenario, we can observe that the initial condition is expressed as $v(\cdot,0) = g$ in the $L^2$-sense.*

3.2. **Identifiability.** The main result of this section is the identifiability of the spatial component $f^* = \chi_{\mathcal{D}^*}$ in problem (2) from the boundary measurement data $\phi$.

**Theorem 9.** *(Uniqueness). Let $\zeta \in L^2(0,T)$ be a non-null function, and let $\varphi \in L^2(0,T;L^2(\partial\Omega))$. For $\ell = \{1,2\}$, let $f_\ell^* = \chi_{\mathcal{D}_\ell^*}$ be such that the solutions $\boldsymbol{u}_\ell$ of the problems*

$$\left\{\begin{array}{rcll} \partial_t^\alpha \boldsymbol{u}_\ell - \Delta\boldsymbol{u}_\ell + \boldsymbol{u}_\ell &=& \zeta\, f_\ell^* & \text{in } (0,\,T)\times\Omega,\\ \boldsymbol{u}_\ell &=& \varphi & \text{on } (0,\,T)\times\partial\Omega,\\ \boldsymbol{u}_\ell(.,0) &=& 0 & \text{in } \Omega, \end{array}\right.$$

*satisfy*

$$\partial_\nu \boldsymbol{u}_1 = \partial_\nu \boldsymbol{u}_2 = \phi \quad \text{on } (0,\,T)\times\partial\Omega. \tag{28}$$

*Then we have $f_1^* = f_2^*$, i.e. $\mathcal{D}_1^* = \mathcal{D}_2^*$.*

*Proof.* We define $\boldsymbol{u}_{2,1} = \boldsymbol{u}_2 - \boldsymbol{u}_1$ from which we have the following system:

$$\left\{\begin{array}{rcll} \partial_t^\alpha \boldsymbol{u}_{2,1} - \Delta\boldsymbol{u}_{2,1} + \boldsymbol{u}_{2,1} &=& \zeta\left(f_2^* - f_1^*\right) & \text{in } (0,\,T)\times\Omega,\\ \boldsymbol{u}_{2,1} &=& 0 & \text{on } (0,\,T)\times\partial\Omega,\\ \boldsymbol{u}_{2,1}(.,0) &=& 0 & \text{in } \Omega. \end{array}\right. \tag{29}$$

According to (28), we have

$$\partial_\nu \boldsymbol{u}_{2,1} = 0 \quad \text{on } (0,\,T)\times\partial\Omega. \tag{30}$$

By Theorem 4.1 from [32], the problem (29) admits a unique weak solution in the sense of [32, Definition 4.1] and satisfying the regularity property:

$$\boldsymbol{u}_{2,1} \in H_\alpha(0,T;L^2(\Omega)) \cap L^2(0,T;H^2(\Omega)\cap H_0^1(\Omega)). \tag{31}$$

We set $\boldsymbol{w} := J_{1-\alpha}\boldsymbol{u}_{2,1}$. In terms of Lemma 7, we have

$$\boldsymbol{w}(t,\cdot) = \int_0^t \zeta(\tau)\, v(t-\tau,\cdot)\mathrm{d}\tau \quad \text{in} \quad \Omega,\ 0<t<T, \tag{32}$$

where $v$ is the solution of (23) with $f_{2,1}^* = \Big(f_2^* - f_1^*\Big)$ in place of $g$. Differentiating two sides of equality (32) with respect to $x \in \partial\Omega$, we get

$$\partial_\nu \boldsymbol{w}(t,\cdot) = \int_0^t \zeta(\tau)\, \partial_\nu v(t-\tau,\cdot)\mathrm{d}\tau \quad \text{on} \quad \partial\Omega,\ 0<t<T.$$

Moreover, according to (30), we have $\partial_\nu \boldsymbol{w} = J_{1-\alpha}\big(\partial_\nu \boldsymbol{u}_{2,1}\big) = 0$ on $(0,T)\times\partial\Omega$. Consequently,

$$\int_0^t \zeta(\tau)\, \partial_\nu v(t-\tau,\cdot)\mathrm{d}\tau = 0 \quad \text{on} \quad \partial\Omega,\ 0<t<T. \tag{33}$$

From Lemma 5, there exists $t^* \in [0,\, T]$ such that $\zeta = 0$ in $(0,\, T-t^*)$ and $\partial_\nu v = 0$ on $(0,t^*)\times\partial\Omega$. Since $\zeta$ is a given non-null function in $L^2(0,\, T)$, it is easy to deduce that $t^*$ is strictly positive, i.e. we can conclude $t^* > 0$. This implies that $\partial_\nu v(t,\cdot) = 0$ on $\partial\Omega$ for any $t \in I = (0,t^*)$ is nonempty open interval in $\mathbb{R}$. Therefore, the function $v$ in $(0,t^*)\times\Omega$ satisfies the following system

$$\begin{cases} \partial_t^\alpha\Big(v - f_{2,1}^*\Big) - \Delta v + v = 0 \ \text{ in } \ (0,t^*)\times\Omega, \\ \\ v - f_{2,1}^* \in H_\alpha(0,t^*;L^2(\Omega)), \\ \\ v = \partial_\nu v = 0 \ \text{ on } \ (0,t^*)\times\partial\Omega. \end{cases} \tag{34}$$

According to [39, Lemma 2.1], one can deduce that the solution $v$ of the above initial-boundary value problem (34) without the Neumann condition $\partial_\nu v = 0$ can be analytically extended from $(0,t^*)$ to $(0,\infty)$. Using this with the unique continuation result in [40], we have

$$v = 0 \quad \text{in} \quad (0,\infty)\times\Omega.$$

Consequently, we have

$$\partial_t^\alpha\Big(v - f_{2,1}^*\Big) = 0 \quad \text{in} \quad (0,T)\times\Omega.$$

Hence,

$$v - f_{2,1}^* = J_\alpha\big(J_\alpha\big)^{-1}\Big(v - f_{2,1}^*\Big) = J_\alpha\partial_t^\alpha\Big(v - f_{2,1}^*\Big) = 0 \quad \text{in} \quad (0,T)\times\Omega.$$

We know that $v = 0$ in $(0,T)\times\Omega$, then $f_{2,1}^* = 0$ in $\Omega$, which implies $f_2^* = f_1^*$ i.e. $\mathcal{D}_2^* = \mathcal{D}_1^*$. □

## 4. Coupled complex boundary problem

In this section, we aim to reformulate our geometric inverse source problem into a boundary value problem with complex Robin conditions. Our proposed formulation combines the two boundary conditions (Dirichlet and Neumann) on $\partial\Omega$ to create complex Robin-type conditions. This enables us to examine the resulting complex boundary value problem:

$$\begin{cases} \partial_t^\alpha \boldsymbol{u} - \Delta\boldsymbol{u} + \boldsymbol{u} &=& \zeta\,\chi_{\mathcal{D}^*} & \text{in} & (0,T)\times\Omega, \\ \partial_\nu \boldsymbol{u} + \beta\boldsymbol{i}\,\boldsymbol{u} &=& \phi + \beta\boldsymbol{i}\,\varphi & \text{on} & (0,T)\times\partial\Omega, \\ \boldsymbol{u}(.,0) &=& 0 & \text{in} & \Omega, \end{cases} \tag{35}$$

where $\boldsymbol{i}$ is the imaginary number, i.e., $\boldsymbol{i} = \sqrt{-1}$ and $\beta > 0$ is a user defined parameter for numerical purposes [30]. The well-posedness of (35), is guaranteed by the well-known complex

version of the Lax-Milgram lemma (see [22, p. 376]). Assume that $\boldsymbol{u} = u_1 + \boldsymbol{i}\, u_2$ be the unique weak solution of (35). Then real-valued function $(u_1, u_2)$ is a unique solution of the coupled system

$$\left\{\begin{array}{rcll} \partial_t^\alpha u_1 - \Delta u_1 + u_1 &=& \zeta\, \chi_{\mathcal{D}^*} & \text{in} \quad (0,T)\times\Omega, \\ \partial_\nu u_1 - \beta u_2 &=& \phi & \text{on} \quad (0,T)\times\partial\Omega, \\ u_1(.,0) &=& 0 & \text{in} \quad \Omega, \end{array}\right. \tag{36}$$

$$\left\{\begin{array}{rcll} \partial_t^\alpha u_2 - \Delta u_2 + u_2 &=& 0 & \text{in} \quad (0,T)\times\Omega, \\ \partial_\nu u_2 + \beta u_1 &=& \beta\varphi & \text{on} \quad (0,T)\times\partial\Omega, \\ u_2(.,0) &=& 0 & \text{in} \quad \Omega. \end{array}\right. \tag{37}$$

We observe that if $u_2 = 0$ in $(0,\, T)\times\Omega$, then $u_2 = 0$ and $\partial_\nu u_2 = 0$ on $(0,\, T)\times\partial\Omega$. Consequently, from the boundary value problems (36) and (37), we can conclude that $u_1$ is a solution of the overdetermined boundary problem (1)-(3).

Conversely, if $\boldsymbol{u}$ is the unique solution of the overdetermined problem (1)-(3), then the unique weak solution of (36), $u_1$, is equal to $\boldsymbol{u}$ almost everywhere in $(0,T)\times\Omega$ and the unique weak solution of (37), $u_2$, is equal to 0 almost everywhere in $(0,T)\times\Omega$.

Based on this observation, we can conclude that the problem of reconstructing the spatial component of the source term $f^* = \chi_{\mathcal{D}^*}$ is equivalent to the following problem:

**Inverse Problem Reformulation :** Find $f = \chi_{\mathcal{D}} \in \mathcal{A}(\Omega)$ such that the imaginary part of $\boldsymbol{u}[f]$, $\mathfrak{I}\big\{\boldsymbol{u}[f]\big\} = 0$ in $(0,T)\times\Omega$, where $\boldsymbol{u}[f]$ being the unique weak solution of the probelm

$$\left\{\begin{array}{rcll} \partial_t^\alpha \boldsymbol{u}[f] - \Delta \boldsymbol{u}[f] + \boldsymbol{u}[f] &=& \zeta\, f & \text{in} \quad (0,T)\times\Omega, \\ \partial_\nu \boldsymbol{u}[f] + \beta \boldsymbol{i}\, \boldsymbol{u}[f] &=& \phi + \beta \boldsymbol{i}\, \varphi & \text{on} \quad (0,T)\times\partial\Omega, \\ \boldsymbol{u}[f](.,0) &=& 0 & \text{in} \quad \Omega. \end{array}\right. \tag{38}$$

Here $\mathcal{A}(\Omega)$ is the set of admissible solutions. It contains the characteristic functions having the form

$$\mathcal{A}(\Omega) = \Big\{ f \in L^\infty(\Omega) :\ f = \chi_{\mathcal{D}},\ \mathcal{D} \subset\subset \Omega \Big\}, \tag{39}$$

where $\mathcal{D}$ is an open set having a uniform Lipschitz boundary $\partial\mathcal{D}$ in the sense of [33, Definition 2.4.5].

**Optimization Problem :** To solve the reformulated inverse shape problem, we transform it into a shape optimization problem. Define a functional

$$\mathcal{K}(f) = \int_0^T \int_\Omega \Big| u_2[f] \Big|^2 \mathrm{d}x\mathrm{d}t, \tag{40}$$

and introduce the minimization problem :

Find $f^* = \chi_{\mathcal{D}^*} \in \mathcal{A}(\Omega)$, such that

$$\mathcal{K}(f^*) = \underset{f=\chi_{\mathcal{D}}\in\mathcal{A}(\Omega)}{\text{Minimize}}\ \mathcal{K}(f). \tag{41}$$

In (40), $u_2[f]$ represents the imaginary part of $\boldsymbol{u}[f]$, the unique weak solution of (38). It is well known that this problem is unstable under data perturbations, with the solution being very sensitive to the measured data. This sensitivity can cause severe numerical instabilities. To address the issue of well-posedness for the minimization problem (41), a possible approach is to incorporate a Tikhonov regularization term in the functional to be minimized (see, e.g., [17]). This can be achieved by adding a penalization term for the perimeter of the subdomain $\mathcal{D}$, resulting in the following regularized shape functional:

$$\mathcal{K}_\eta(f) = \int_0^T \int_\Omega \Big| u_2[f] \Big|^2 \mathrm{d}x\mathrm{d}t + \eta\, P_\Omega(\mathcal{D}), \tag{42}$$

where $\eta > 0$ is a parameter in the regularization term.

Through this regularization process, the reconstruction problem of the spatial source $f^* = \chi_{\mathcal{D}^*}$ from boundary measurements can be reformulated as a regularized optimization problem. The unknown spatial characteristic function $f^* = \chi_{\mathcal{D}^*}$ can be characterized as the solution to the following minimization problem

$$\underset{f=\chi_{\mathcal{D}}\in\mathcal{A}(\Omega)}{\text{Minimize}}\ \mathcal{K}_\eta(f). \tag{43}$$

To conclude this section, we briefly present some useful properties of the perimeter $P_\Omega$. For more information, the reader may refer to [33]. For a Lipschitz domain $\mathcal{D}$, the perimeter of the domain is equal to the 1-dimensional Hausdorff measure $\mathcal{H}^1$ of its boundary $\partial\mathcal{D}$; i.e.

$$P_\Omega(\mathcal{D}) = \mathcal{H}^1(\partial\mathcal{D}).$$

Moreover, when $P_\Omega(\mathcal{D}) < \infty$ the relative perimeter $P_\Omega(\mathcal{D})$ coincides with the Total Variation (TV) of the distributional gradient of the characteristic function of $\mathcal{D}$, namely:

$$P_\Omega(\mathcal{D}) = \mathrm{TV}\Big(\chi_{\mathcal{D}}, \Omega\Big) = |\nabla\chi_{\mathcal{D}}|(\Omega). \tag{44}$$

Before discussing the mathematical analysis of our optimization problem (43), we first study the well-posedness of the forward complex problem (38). To simplify further analysis, we set $\beta = 1$ in Sections 4.1-6.

4.1. **Well-posedness of the forward complex problem.** In this section, we will prove the existence and uniqueness of weak solutions for the forward complex problem (38). To introduce the concept of weak solutions to (38), for $0 < \alpha < 1$, we define a space

$$B^\alpha(\Omega) := H_\alpha(0,T;L^2(\Omega)) \cap L^2(0,T;H^1(\Omega)) \tag{45}$$

equipped with the norm

$$\Big\|\kappa\Big\|^2_{B^\alpha(\Omega)} = \Big\|\kappa\Big\|^2_{H^\alpha(0,T;L^2(\Omega))} + \Big\|\kappa\Big\|^2_{L^2(0,T;H^1(\Omega))}. \tag{46}$$

As stated in reference [54], it is known that $B^{\frac{\alpha}{2}}(\Omega)$ is a Hilbert space. We will now introduce the complex version of $B^\alpha(\Omega)$, denoted as $\mathbf{B}^\alpha(\Omega) = B^\alpha(\Omega) \oplus \boldsymbol{i}\, B^\alpha(\Omega)$ equipped with the norm

$$\Big|\Big|\Big|\boldsymbol{v}\Big|\Big|\Big|^2_{\mathbf{B}^\alpha(\Omega)} = \Big\|v_1\Big\|^2_{B^\alpha(\Omega)} + \Big\|v_2\Big\|^2_{B^\alpha(\Omega)} \quad \text{for all } \ \boldsymbol{v} = v_1 + \boldsymbol{i}\, v_2 \in \mathbf{B}^\alpha(\Omega). \tag{47}$$

**Definition 10.** *(see* [51]*). Let* $\kappa : \mathbb{R}_+ \longrightarrow \mathbb{R}$*, then for* $0 < \alpha < 1$*, the Riemann-Liouville fractional left-sided derivative* $D^\alpha_{0^+}$ *and right-sided derivative* $D^\alpha_{T^-}$ *of order* $\alpha$ *are defined by*

$$D^\alpha_{0^+}\kappa(t) = \frac{1}{\Gamma(1-\alpha)}\frac{d}{dt}\int_0^t (t-\tau)^{-\alpha}\kappa(\tau)\mathrm{d}\tau, \quad 0 \le t \le T, \tag{48}$$

$$D^\alpha_{T^-}\kappa(t) = \frac{-1}{\Gamma(1-\alpha)}\frac{d}{dt}\int_t^T (\tau-t)^{-\alpha}\kappa(\tau)\mathrm{d}\tau, \quad 0 \le t \le T. \tag{49}$$

**Lemma 11.** *(see* [53, Lemma 2.5]*). Let* $\kappa \in H^{\frac{\alpha}{2}}(0,T)$*, then for* $0 < \alpha < 1$*,*

$$\Big\|D^{\frac{a}{2}}_{0+}\kappa\Big\|_{L^2(0,T)} \sim \Big\|\kappa\Big\|_{H^{\frac{\alpha}{2}}(0,T)} \sim \Big\|D^{\frac{a}{2}}_{T^-}\kappa\Big\|_{L^2(0,T)}, \tag{50}$$

$$\int_0^T D^{\alpha/2}_{0^+}\kappa\, D^{\alpha/2}_{T^-}\kappa\,\mathrm{d}t \ge \cos\Big(\frac{\pi\alpha}{2}\Big)\Big\|D^{\alpha/2}_{0^+}\kappa\Big\|^2_{L^2(0,T)}, \tag{51}$$

*where the notation* $\sim$ *denotes the norm equivalence.*

Following [54], a weak formulation for problem (38) reads as follows: Find $\boldsymbol{u}[f] \in \mathbf{B}^{\frac{\alpha}{2}}(\Omega)$ such that

$$a(\boldsymbol{u}[f], \boldsymbol{v}) = l(\boldsymbol{v}) \quad \forall \boldsymbol{v} \in \mathbf{B}^{\frac{\alpha}{2}}(\Omega), \tag{52}$$

where the sesquilinear form $a(\cdot,\, \cdot)$ is defined by

$$a(\boldsymbol{w}, \boldsymbol{v}) = \int_0^T \int_\Omega \Big( D_{0^+}^{\alpha/2} \boldsymbol{w}\, D_{T^-}^{\alpha/2} \overline{\boldsymbol{v}} + \nabla \boldsymbol{w} \cdot \nabla \overline{\boldsymbol{v}} + \boldsymbol{w}\, \overline{\boldsymbol{v}} \Big)\, \mathrm{d}x\mathrm{d}t + \boldsymbol{i} \int_0^T \int_{\partial\Omega} \boldsymbol{w}\, \overline{\boldsymbol{v}}\, \mathrm{d}s(x)\mathrm{d}t \;\; \forall \boldsymbol{w}, \boldsymbol{v} \in \mathbf{B}^{\frac{\alpha}{2}}(\Omega), \tag{53}$$

and the linear form $l(\cdot)$ is given by

$$l(\boldsymbol{v}) = \int_0^T \int_\Omega f\, \zeta\, \overline{\boldsymbol{v}}\, \mathrm{d}x\mathrm{d}t + \int_0^T \int_{\partial\Omega} \phi\, \overline{\boldsymbol{v}}\, \mathrm{d}s(x)\mathrm{d}t + \boldsymbol{i} \int_0^T \int_{\partial\Omega} \varphi\, \overline{\boldsymbol{v}}\, \mathrm{d}s(x)\mathrm{d}t \quad \forall \boldsymbol{v} \in \mathbf{B}^{\frac{\alpha}{2}}(\Omega). \tag{54}$$

Here, $\overline{(\cdot)}$ represents the complex conjugate of $(\cdot)$.

In the following theorem, we demonstrate existence and uniqueness result for the complex time-fractional diffusion problem (38).

**Theorem 12.** *Given $f \in L^2(\Omega)$, $\zeta \in L^2(0,\, T)$, $\varphi \in L^2(0, T; L^2(\partial\Omega))$, and $\phi \in L^2(0, T; L^2(\partial\Omega))$, problem (38) has a unique weak solution. Moreover, there exists a constant $C(\alpha) > 0$ such that*

$$\Big|\Big|\Big| \boldsymbol{u}[f] \Big|\Big|\Big|_{\mathbf{B}^{\frac{\alpha}{2}}(\Omega)} \leq C(\alpha) \Big( \Big\| f \Big\|_{L^2(\Omega)} + \Big\| \varphi \Big\|_{L^2(0,T;L^2(\partial\Omega))} + \Big\| \phi \Big\|_{L^2(0,T;L^2(\partial\Omega))} \Big). \tag{55}$$

*Proof.* The well-posed of problem (38) is guaranteed by the well-known complex version of the Lax-Milgram lemma (see, for example, [22, p. 376]). More precisely, we show that the sesquilinear form $a(\cdot,\, \cdot)$ is continuous and elliptic on $\mathbf{B}^{\frac{\alpha}{2}}(\Omega)$, and the linear form $l(\cdot)$ is continuous on $\mathbf{B}^{\frac{\alpha}{2}}(\Omega)$.

- Continuity of $a(\cdot,\, \cdot)$ on $\mathbf{B}^{\frac{\alpha}{2}}(\Omega) \times \mathbf{B}^{\frac{\alpha}{2}}(\Omega)$: For any $\boldsymbol{w} = w_1 + \boldsymbol{i}\, w_2$, $\boldsymbol{v} = v_1 + \boldsymbol{i}\, v_2 \in \mathbf{B}^{\frac{\alpha}{2}}(\Omega)$ we have

$$a(\boldsymbol{w},\, \boldsymbol{v}) = \Re\Big\{ a(\boldsymbol{w}, \boldsymbol{v}) \Big\} + \boldsymbol{i}\, \Im\Big\{ a(\boldsymbol{w}, \boldsymbol{v}) \Big\}, \tag{56}$$

where the real and imaginary parts of $a(\boldsymbol{w}, \boldsymbol{v})$ are given by

$$\begin{aligned}
\Re\Big\{ a(\boldsymbol{w}, \boldsymbol{v}) \Big\} &= \int_0^T \int_\Omega \Big( D_{0^+}^{\alpha/2} w_1\, D_{T^-}^{\alpha/2} v_1 + \nabla w_1 \cdot \nabla v_1 + w_1\, v_1 \Big)\, \mathrm{d}x\mathrm{d}t \\
&\quad + \int_0^T \int_\Omega \Big( D_{0^+}^{\alpha/2} w_2\, D_{T^-}^{\alpha/2} v_2 + \nabla w_2 \cdot \nabla v_2 + w_2\, v_2 \Big)\, \mathrm{d}x\mathrm{d}t + \int_0^T \int_{\partial\Omega} \Big( w_1\, v_2 - w_2\, v_1 \Big)\, \mathrm{d}s(x)\mathrm{d}t, \\
\Im\Big\{ a(\boldsymbol{w}, \boldsymbol{v}) \Big\} &= \int_0^T \int_\Omega \Big( D_{0^+}^{\alpha/2} w_2\, D_{T^-}^{\alpha/2} v_1 + \nabla w_2 \cdot \nabla v_1 + w_2\, v_1 \Big)\, \mathrm{d}x\mathrm{d}t \\
&\quad - \int_0^T \int_\Omega \Big( D_{0^+}^{\alpha/2} w_1\, D_{T^-}^{\alpha/2} v_2 + \nabla w_1 \cdot \nabla v_2 + w_1\, v_2 \Big)\, \mathrm{d}x\mathrm{d}t + \int_0^T \int_{\partial\Omega} \Big( w_1\, v_1 + w_2\, v_2 \Big)\, \mathrm{d}s(x)\mathrm{d}t.
\end{aligned}$$

Consequently,

$$\Big| a(\boldsymbol{w}, \boldsymbol{v}) \Big|^2 = \Big( \Re\Big\{ a(\boldsymbol{w}, \boldsymbol{v}) \Big\} \Big)^2 + \Big( \Im\Big\{ a(\boldsymbol{w}, \boldsymbol{v}) \Big\} \Big)^2. \tag{57}$$

On the other hand, by using Cauchy-Schwarz and Hölder inequalities, $(x + y)^2 \leq 2(x^2 + y^2)$ inequality, Lemma 11, and the trace inequality, we can obtain

$$\begin{aligned}
\Big| \Re\Big\{ a(\boldsymbol{w}, \boldsymbol{v}) \Big\} \Big| &\leq C \Big|\Big|\Big| \boldsymbol{w} \Big|\Big|\Big|_{\mathbf{B}^{\frac{\alpha}{2}}(\Omega)} \Big|\Big|\Big| \boldsymbol{v} \Big|\Big|\Big|_{\mathbf{B}^{\frac{\alpha}{2}}(\Omega)}, \\
\Big| \Im\Big\{ a(\boldsymbol{w}, \boldsymbol{v}) \Big\} \Big| &\leq C \Big|\Big|\Big| \boldsymbol{w} \Big|\Big|\Big|_{\mathbf{B}^{\frac{\alpha}{2}}(\Omega)} \Big|\Big|\Big| \boldsymbol{v} \Big|\Big|\Big|_{\mathbf{B}^{\frac{\alpha}{2}}(\Omega)}.
\end{aligned}$$

Inserting the above inequalities into (57), we obtain

$$\Big| a(\boldsymbol{w}, \boldsymbol{v}) \Big| \leq C \Big|\Big|\Big| \boldsymbol{w} \Big|\Big|\Big|_{\mathbf{B}^{\frac{\alpha}{2}}(\Omega)} \Big|\Big|\Big| \boldsymbol{v} \Big|\Big|\Big|_{\mathbf{B}^{\frac{\alpha}{2}}(\Omega)}.$$

Hence, the sesquilinear form $a$ is continuous on $\mathbf{B}^{\frac{\alpha}{2}}(\Omega) \times \mathbf{B}^{\frac{\alpha}{2}}(\Omega)$.

Similarly, we have the continuity of the linear form $l(\cdot)$ :

$$\Big|l(\boldsymbol{v})\Big| \leq C_0\Big(\Big\|f\Big\|_{L^2(\Omega)} + \Big\|\varphi\Big\|_{L^2(0,T;L^2(\partial\Omega))} + \Big\|\phi\Big\|_{L^2(0,T;L^2(\partial\Omega))}\Big)\Big|\Big|\Big|\boldsymbol{v}\Big|\Big|\Big|_{\mathbf{B}^{\frac{\alpha}{2}}(\Omega)}. \tag{58}$$

- Coercivity of $a(\cdot,\,\cdot)$. From (56), one can deduce that:

$$\begin{aligned}\mathfrak{R}\Big\{a(\boldsymbol{v},\boldsymbol{v})\Big\} &= \int_0^T\int_\Omega D_{0^+}^{\alpha/2}v_1\, D_{T^-}^{\alpha/2}v_1\,\mathrm{d}x\mathrm{d}t + \int_0^T\int_\Omega \Big|\nabla v_1\Big|^2\mathrm{d}x\mathrm{d}t + \int_0^T\int_\Omega \Big|v_1\Big|^2\mathrm{d}x\mathrm{d}t\\ &\quad + \int_0^T\int_\Omega D_{0^+}^{\alpha/2}v_2\, D_{T^-}^{\alpha/2}v_2\,\mathrm{d}x\mathrm{d}t + \int_0^T\int_\Omega \Big|\nabla v_2\Big|^2\mathrm{d}x\mathrm{d}t + \int_0^T\int_\Omega \Big|v_2\Big|^2\mathrm{d}x\mathrm{d}t\end{aligned}$$

for all $\boldsymbol{v} = v_1 + \boldsymbol{i}\, v_2 \in \mathbf{B}^{\frac{\alpha}{2}}(\Omega)$. Denote $C_1 = \cos\Big(\dfrac{\pi\alpha}{2}\Big) > 0$ and according to Lemma 11, we get

$$\begin{aligned}\mathfrak{R}\Big\{a(\boldsymbol{v},\boldsymbol{v})\Big\} &\geq C_1\Big\|D_{0^+}^{\alpha/2}v_1\Big\|^2_{L^2(0,T;L^2(\Omega))} + \Big\|v_1\Big\|^2_{L^2(0,T;H^1(\Omega))}\\ &\quad + C_1\Big\|D_{0^+}^{\alpha/2}v_2\Big\|^2_{L^2(0,T;L^2(\Omega))} + \Big\|v_2\Big\|^2_{L^2(0,T;H^1(\Omega))}\\ &\geq C_\alpha\Big\|v_1\Big\|^2_{H^{\frac{\alpha}{2}}(0,T;L^2(\Omega))} + \Big\|v_1\Big\|^2_{L^2(0,T;H^1(\Omega))}\\ &\quad + C_\alpha\Big\|v_2\Big\|^2_{H^{\frac{\alpha}{2}}(0,T;L^2(\Omega))} + \Big\|v_2\Big\|^2_{L^2(0,T;H^1(\Omega))}\\ &\geq \min\Big(C_\alpha,\,1\Big)\Big[\Big\|v_1\Big\|^2_{B^{\frac{\alpha}{2}}(\Omega)} + \Big\|v_2\Big\|^2_{B^{\frac{\alpha}{2}}(\Omega)}\Big] = \min\Big(C_\alpha,\,1\Big)\Big|\Big|\Big|\boldsymbol{v}\Big|\Big|\Big|^2_{\mathbf{B}^{\frac{\alpha}{2}}(\Omega)},\end{aligned}$$

which implies the coercivity of $a(\cdot,\,\cdot)$.

Consequently, according to the complex version of the Lax-Milgram lemma, there exists a unique weak solution $\boldsymbol{u}[f] \in \mathbf{B}^{\frac{\alpha}{2}}(\Omega)$ to (38).

To obtain the stability estimate (55), we can take $\boldsymbol{v} = \boldsymbol{u}[f]$ as a test function in (52) and use the advantage of the fact that $\mathfrak{R}\Big\{a(\boldsymbol{v},\boldsymbol{v})\Big\} \leq \Big|a(\boldsymbol{v},\boldsymbol{v})\Big|$ and the above-mentioned coercivity inequality, along with equation (58), to derive it.

$$\Big|\Big|\Big|\boldsymbol{u}[f]\Big|\Big|\Big|_{\mathbf{B}^{\frac{\alpha}{2}}(\Omega)} \leq C(\alpha)\Big(\Big\|f\Big\|_{L^2(\Omega)} + \Big\|\varphi\Big\|_{L^2(0,T;L^2(\partial\Omega))} + \Big\|\phi\Big\|_{L^2(0,T;L^2(\partial\Omega))}\Big)$$

with $C(\alpha) = \dfrac{C_0}{\min\Big(C_\alpha, 1\Big)}$. □

**Remark 13.** *Note that solving problem* (52) *does not imply satisfying the homogeneous initial condition (i.e.* $\boldsymbol{u}[f](\cdot,\,0) = 0$ *in* $\Omega$*) required by the strong solution of the complex boundary problem* (38)*. This is because functions in the space* $\mathbf{B}^{\frac{\alpha}{2}}(\Omega)$ *with* $\frac{\alpha}{2} < \frac{1}{2}$ *have no trace at time* $t = 0$*. In fact, defining pointwise values (at a given time) of a function in* $B^{\frac{\alpha}{2}}(\Omega)$ *(particularly in the space* $H^{\frac{\alpha}{2}}(0,\,T)$*) with* $\frac{\alpha}{2} < \frac{1}{2}$ *does not make sense (see, for example,* [56]*). Therefore the equivalence between* (38) *and* (52) *should be understood in the sense of a "regular enough solution" (of the real and imaginary parts). Hence, in this case, defining initial values at time* $t = 0$ *makes sense.*

4.2. **Continuity property of solutions with respect to space-dependent source.** In this section, we will prove the continuity of the map $f \longmapsto \boldsymbol{u}[f]$ for functions in the class $\mathcal{A}(\Omega)$ (see (39)) where $\boldsymbol{u}[f]$ is the solution to the forward complex problem (38). For this purpose, we review the definition of convergence in the sense of characteristic functions and highlight its key properties.

**Definition 14.** *(see* [33, Definition 2.2.3]*). Let* $\{D_n\}_{n\geq 1}$ *and* $D$ *be measurable sets of* $\mathbb{R}^2$*. It is said that* $D_n \longrightarrow D$ *in the sense of characteristic functions as* $n \to \infty$ *if*

$$\chi_{D_n} \longrightarrow \chi_D \quad \text{in } L^p_{loc}(\mathbb{R}^2) \quad \text{for all } \ p \in [1, +\infty[. \tag{59}$$

**Remark 15.** *In the above convergence result* (59)*, we can take any* $p < \infty$ *since, as* $|\chi_{D^n} - \chi_D|$ *only takes on the values* 0 *and* 1*, we have, for any finite* $p$*,*

$$|\chi_{D_n} - \chi_D|^p = |\chi_{D_n} - \chi_D| \quad \text{which implies that} \quad \|\chi_{D_n} - \chi_D\|_{L^p} = \|\chi_{D_n} - \chi_D\|_{L^1}^{1/p}.$$

*On the other hand, the case* $p = \infty$ *has no interest since* $\|\chi_{D_n} - \chi_D\|_{L^\infty} = 1$ *as soon as* $D^n$ *and* $D$ *different on a set of non-zero measure.*

The uniform Lipschitz boundary condition of the subdomain $\mathcal{D}$ is a relevant requirement in the set of admissible solutions $\mathcal{A}(\Omega)$ for the existence of optimal solutions to our optimization problem (43). Specifically, according to [33, Theorem 2.4.10], this condition ensures that the set of admissible solutions $\mathcal{A}(\Omega)$ has the following compactness property:

**Lemma 16.** *The class* $\mathcal{A}(\Omega)$ *is compact with respect to the topology of characteristic functions.*

We can now prove the following continuity result.

**Theorem 17.** *Let* $\{f_n = \chi_{\mathcal{D}_n}\}_n \subset \mathcal{A}(\Omega)$ *be a sequence of sets converging to* $f^* = \chi_{\mathcal{D}^*}$ *in the sense of characteristic functions (cf. Lemma 16), and let* $\boldsymbol{u}[f_n] \in \mathbf{B}^{\frac{\alpha}{2}}(\Omega)$, $\boldsymbol{u}[f^*] \in \mathbf{B}^{\frac{\alpha}{2}}(\Omega)$ *be solutions of* (38) *with space-dependent source term* $f_n = \chi_{\mathcal{D}_n}$, $f^* = \chi_{\mathcal{D}^*}$*, respectively. Then*

$$\lim_{n\longrightarrow\infty} \Big|\Big|\Big| \boldsymbol{u}[f_n] - \boldsymbol{u}[f^*] \Big|\Big|\Big|_{\mathbf{B}^{\frac{\alpha}{2}}(\Omega)} = 0. \tag{60}$$

*Proof.* Consider the difference $\boldsymbol{U}_n = \boldsymbol{u}[f_n] - \boldsymbol{u}[f^*]$, which is the solution to

$$\left\{ \begin{array}{rcll} \partial_t^\alpha \boldsymbol{U}_n - \Delta \boldsymbol{U}_n + \boldsymbol{U}_n &=& \zeta\left(f_n - f^*\right) & \text{in} \quad (0,T)\times\Omega, \\ \partial_\nu \boldsymbol{U}_n + \boldsymbol{i}\,\boldsymbol{U}_n &=& 0 & \text{on} \quad (0,T)\times\partial\Omega, \\ \boldsymbol{U}_n(.,0) &=& 0 & \text{in} \quad \Omega. \end{array} \right. \tag{61}$$

By repeating the same argument as in the proof of estimate (55) and utilizing Remark 15, we can derive

$$\begin{aligned} \Big|\Big|\Big| \boldsymbol{U}_n \Big|\Big|\Big|_{\mathbf{B}^{\frac{\alpha}{2}}(\Omega)} &\leq C(\alpha) \Big\| f_n - f^* \Big\|_{L^2(\Omega)} \\ &\leq C(\alpha) \Big\| f_n - f^* \Big\|_{L^1(\Omega)}^{\frac{1}{2}}. \end{aligned}$$

From the convergence of $\mathcal{D}_n$ to $\mathcal{D}^*$ in the sense of characteristic functions as $n \longrightarrow \infty$, we obtain

$$\Big|\Big|\Big| \boldsymbol{U}_n \Big|\Big|\Big|_{\mathbf{B}^{\frac{\alpha}{2}}(\Omega)} \longrightarrow 0 \quad \text{as} \quad n \to \infty.$$

□

Based on this continuity result, we will analyze some theoretical results regarding solutions to the optimization problem in the following section.

## 5. Well-posedness of the optimization problem

In this section, we present three key theoretical results related to the regularized optimization problem (43). The first result establishes the existence of an optimal solution, the second addresses its stability.

5.1. **Existence of an optimal solution.** The objective of this section is to establish the existence of an optimal solution to the optimization problem under investigation.

**Theorem 18.** *For every $\eta > 0$ there exists $f^* = \chi_{\mathcal{D}^*} \in \mathcal{A}(\Omega)$ such that*

$$\mathcal{K}_\eta(f^*) = \inf\Big\{\mathcal{K}_\eta(f), \quad f \in \mathcal{A}(\Omega)\Big\}.$$

*Proof.* The functional $\mathcal{K}_\eta$ is bounded from below by zero, so that there exists a minimizing sequence $\Big\{f_n = \chi_{\mathcal{D}_n}\Big\}_n \subset \mathcal{A}(\Omega)$ decreasing in $\mathcal{K}_\eta$ and satisfying

$$\lim_{n\longrightarrow\infty} \mathcal{K}_\eta(f_n) = \inf_{f\in\mathcal{A}(\Omega)} \mathcal{K}_\eta(f).$$

By the compactness of $\mathcal{A}(\Omega)$ established in Lemma 16, there exist an open set $\mathcal{D}^* \subset \Omega$ with a uniform Lipschitz boundary $\partial\mathcal{D}^*$, and a subsequence of $\Big\{\mathcal{D}_n\Big\}_n$ (which we still label by $n$) that converges to $\mathcal{D}^*$ in the sense of characteristic functions; i.e.

$$f_n = \chi_{\mathcal{D}_n} \longrightarrow f^* = \chi_{\mathcal{D}^*} \text{ in } L^1(\Omega) \text{ as } n \to \infty.$$

We now show that $f^* = \chi_{\mathcal{D}^*} \in \mathcal{A}(\Omega)$ is a minimizer for (43). For each $n \in \mathbb{N}$, we consider $\boldsymbol{u}[f_n]$, which is the solution of the complex time-fractional diffusion problem (38) with $f_n$ in place of $f$.
By applying Theorem 17, we can conclude that

$$\Big|\Big|\Big|\boldsymbol{u}[f_n]\Big|\Big|\Big|_{\mathbf{B}^{\frac{\alpha}{2}}(\Omega)} \longrightarrow \Big|\Big|\Big|\boldsymbol{u}[f^*]\Big|\Big|\Big|_{\mathbf{B}^{\frac{\alpha}{2}}(\Omega)} \text{ as } n \to \infty. \tag{62}$$

We define $u_2[f_n]$ as the imaginary part of the complex-valued function $\boldsymbol{u}[f_n]$, and $u_2[f^*]$ as the imaginary part of $\boldsymbol{u}[f^*]$. Consequently, by using (62), we can deduce that

$$\Big|\Big|u_2[f_n]\Big|\Big|_{L^2(0,T;L^2(\Omega))} \longrightarrow \Big|\Big|u_2[f^*]\Big|\Big|_{L^2(0,T;L^2(\Omega))} \text{ as } n \to \infty. \tag{63}$$

Since the perimeter $P_\Omega$ is lower semi-continuous with respect to the convergence of characteristic functions (see, for example, [33]),

$$P_\Omega(\mathcal{D}^*) \leq \liminf_{n\to\infty} P_\Omega(\mathcal{D}_n). \tag{64}$$

Furthermore, it is well-known that the $L^2$-norm is lower semi-continuous. By combining these results, we can establish the lower semi-continuity of the cost function $\mathcal{K}_\eta$. Finally, by combining the lower semi-continuity of $\mathcal{K}_\eta$ with the convergence result (63), we can deduce

$$\mathcal{K}_\eta(f^*) \leq \liminf_{n\to\infty} \mathcal{K}_\eta(f_n)$$

which implies

$$\mathcal{K}_\eta(f^*) = \inf_{f\in\mathcal{A}(\Omega)} \mathcal{K}_\eta(f),$$

i.e. $f^* = \chi_{\mathcal{D}^*}$ is a solution of the minimization problem (43). The proof of Theorem 18 is completed. □

The previous result (Theorem 18) ensures the existence of an optimal solution for problem (43), however, the uniqueness of the minimizer cannot be guaranteed due to the non-linear and non-convex of the functional $\mathcal{K}_\eta$. It is worth noting that the question of uniqueness remains unresolved.

Next, we want to investigate the stable dependance of the minimizers of the functional $\mathcal{K}_\eta$ on the error level.

5.2. **Stability.** In this study, we examine the stability of the minimizer of the regularized shape functional $\mathcal{K}_\eta$ with respect to small perturbations of the measurement data $\phi$. To check these issues, let us define $\{\phi_n\}_n$ as a sequence of "measurements" in $L^2(0,T;L^2(\partial\Omega))$, such that

$$\Big\|\phi_n - \phi\Big\|_{L^2(0,T;L^2(\partial\Omega))} \longrightarrow 0 \ \text{ as } n \to \infty. \tag{65}$$

To simplify further analysis, we denote by $u_2[f,\phi_n]$ the imaginary part of $\boldsymbol{u}[f,\phi_n]$, where $\boldsymbol{u}[f,\phi_n] = u_1[f,\phi_n] + \boldsymbol{i}\, u_2[f,\phi_n]$ is the solution of the following complex boundary problem:

$$\left\{\begin{array}{rcll} \partial_t^\alpha \boldsymbol{u}[f,\phi_n] - \Delta \boldsymbol{u}[f,\phi_n] + \boldsymbol{u}[f,\phi_n] &=& \zeta\, f & \text{in } (0,T)\times\Omega, \\ \partial_\nu \boldsymbol{u}[f,\phi_n] + \boldsymbol{i}\,\boldsymbol{u}[f,\phi_n] &=& \phi_n + \boldsymbol{i}\,\varphi & \text{on } (0,T)\times\partial\Omega, \\ \boldsymbol{u}[f,\phi_n](.,0) &=& 0 & \text{in } \Omega. \end{array}\right. \tag{66}$$

For each $n \in \mathbb{N}$, we denote by $f_n = \chi_{\mathcal{D}_n} \in \mathcal{A}(\Omega)$ the solution to the following perturbed shape optimization problem:

$$\underset{f=\chi_{\mathcal{D}}\in\mathcal{A}(\Omega)}{\text{Minimize}}\ \mathcal{K}_\eta^n(f), \tag{67}$$

where the shape functional $\mathcal{K}_\eta^n(f)$ is defined as

$$\mathcal{K}_\eta^n(f) := \int_0^T \int_\Omega \Big|u_2[f,\phi_n]\Big|^2 \mathrm{d}x\mathrm{d}t + \eta\, P_\Omega(\mathcal{D}). \tag{68}$$

In the upcoming theorem, we investigate the convergence of the sequence $\{f_n = \chi_{\mathcal{D}_n}\}_n$ when the perturbed data $\{\phi_n\}_n$ tends to a given state $\phi$.

**Theorem 19.** *If $\phi_n$ tends to $\phi$ in $L^2(0,T;L^2(\partial\Omega))$ as $n \longrightarrow \infty$. Then there exists a subsequence of $\{f_n = \chi_{\mathcal{D}_n}\}_n$, such that*

$$f_{n_k} = \chi_{\mathcal{D}_{n_k}} \longrightarrow f^* = \chi_{\mathcal{D}^*} \quad \textit{in} \quad L^1(\Omega) \ \textit{as } k \to \infty,$$

*where $f^* = \chi_{\mathcal{D}^*} \in \mathcal{A}(\Omega)$ is a minimizer of the optimization problem (43), with datum $\phi$.*

*Proof.* The previous Theorem 18 guarantees the existence of each $f_n = \chi_{\mathcal{D}_n}$. Moreover, thanks to the compactness of the sets $\mathcal{A}(\Omega)$ (see Lemma 16), there exists $f^* = \chi_{\mathcal{D}^*} \in \mathcal{A}(\Omega)$ and a sub-sequence, still denoted by $\{f_n = \chi_{\mathcal{D}_n}\}$, such that

$$f_n = \chi_{\mathcal{D}_n} \longrightarrow f^* = \chi_{\mathcal{D}^*} \ \text{ in } \ L^1(\Omega) \ \text{ as } n \to \infty. \tag{69}$$

We will now demonstrate that $f^* = \chi_{\mathcal{D}^*}$ is a minimizer of (67). In order to obtain this result, let us define the following complex-valued function

$$\boldsymbol{w}_n = \boldsymbol{u}[f_n,\phi_n] - \boldsymbol{u}[f^*,\phi],$$

where $\boldsymbol{u}[f^*,\phi]$ is the solution of (66) with $f^*$ and $\phi$ in place of $f_n$ and $\phi_n$, respectively. We can easily deduce that $\boldsymbol{w}_n$ is solution to

$$\left\{\begin{array}{rcll} \partial_t^\alpha \boldsymbol{w}_n - \Delta \boldsymbol{w}_n + \boldsymbol{w}_n &=& \zeta\Big(f_n - f^*\Big) & \text{in } (0,T)\times\Omega, \\ \partial_\nu \boldsymbol{w}_n + \boldsymbol{i}\,\boldsymbol{w}_n &=& \phi_n - \phi & \text{on } (0,T)\times\partial\Omega, \\ \boldsymbol{w}_n(\cdot,0) &=& 0 & \text{in } \Omega. \end{array}\right. \tag{70}$$

Using the same argument as in the proof of (55), we can obtain the following inequality:

$$\begin{aligned} \Big|\Big|\Big|\boldsymbol{w}_n\Big|\Big|\Big|_{\mathbf{B}^{\frac{\alpha}{2}}(\Omega)} &\le C\Big(\Big\|f_n - f^*\Big\|_{L^2(\Omega)} + \Big\|\phi_n - \phi\Big\|_{L^2(0,T;L^2(\partial\Omega))}\Big) \\ &= C\Big(\Big\|f_n - f^*\Big\|^{1/2}_{L^1(\Omega)} + \Big\|\phi_n - \phi\Big\|_{L^2(0,T;L^2(\partial\Omega))}\Big), \end{aligned}$$

where $C$ is a positive constant that depends on $\alpha$. By utilizing the convergence results provided in equations (65) and (69), one can derive

$$\boldsymbol{w}_n \longrightarrow 0 \ \text{ in } \ \mathbf{B}^{\frac{\alpha}{2}}(\Omega) \ \text{ as } n \to \infty. \tag{71}$$

Let us denote by $u_2[f_n,\phi_n]$ the imaginary part of $\boldsymbol{u}[f_n,\phi_n]$, and $u_2[f^*,\phi]$ the imaginary part of $\boldsymbol{u}[f^*,\phi]$. We have

$$u_2[f_n,\phi_n]-u_2[f^*,\phi]\longrightarrow 0 \ \text{ in } \ L^2(0,T;L^2(\Omega)) \ \text{ as } n\to\infty \tag{72}$$

which implies

$$\Big|\Big|u_2[f_n,\phi_n]\Big|\Big|_{L^2(0,T;L^2(\Omega))}\longrightarrow \Big|\Big|u_2[f^*,\phi]\Big|\Big|_{L^2(0,T;L^2(\Omega))} \quad \text{as } n\to\infty. \tag{73}$$

By following the same procedure used in the proof of (73), we can deduce that for any $f\in\mathcal{A}(\Omega)$,

$$\Big|\Big|u_2[f,\phi_n]\Big|\Big|_{L^2(0,T;L^2(\Omega))}\longrightarrow \Big|\Big|u_2[f,\phi]\Big|\Big|_{L^2(0,T;L^2(\Omega))} \quad \text{as } n\to\infty, \tag{74}$$

Finally, we can use the convergence results (73) and (74), along with the lower semi-continuity of both the $L^2$-norm and the perimeter, to show that for any $f=\chi_{\mathcal{D}}\in\mathcal{A}(\Omega)$, we obtain

$$\begin{aligned}
\mathcal{K}_\eta(f^*=\chi_{\mathcal{D}^*}) &= \int_0^T\int_\Omega \Big|u_2[f^*]\Big|^2\mathrm{d}x\mathrm{d}t+\eta\,P_\Omega(\mathcal{D}^*)\\
&= \int_0^T\int_\Omega \Big|u_2[f^*,\phi]\Big|^2\mathrm{d}x\mathrm{d}t+\eta\,P_\Omega(\mathcal{D}^*)\\
&\le \liminf_{n\to\infty}\int_0^T\int_\Omega \Big|u_2[f_n,\phi_n]\Big|^2\mathrm{d}x\mathrm{d}t+\eta\liminf_{n\to\infty}P_\Omega(\mathcal{D}_n)\\
&\le \liminf_{n\to\infty}\Big(\int_0^T\int_\Omega \Big|u_2[f_n,\phi_n]\Big|^2\mathrm{d}x\mathrm{d}t+\eta\,P_\Omega(\mathcal{D}_n)\Big)\\
&\le \lim_{n\to\infty}\Big(\int_0^T\int_\Omega \Big|u_2[f,\phi_n]\Big|^2\mathrm{d}x\mathrm{d}t+\eta\,P_\Omega(\mathcal{D})\Big)\\
&= \int_0^T\int_\Omega \Big|u_2[f,\phi]\Big|^2\mathrm{d}x\mathrm{d}t+\eta\,P_\Omega(\mathcal{D})\\
&= \int_0^T\int_\Omega \Big|u_2[f]\Big|^2\mathrm{d}x\mathrm{d}t+\eta\,P_\Omega(\mathcal{D})=\mathcal{K}_\eta(f) \quad \text{for all } \ f\in\mathcal{A}(\Omega),
\end{aligned}$$

which verifies that $f^*=\chi_{\mathcal{D}^*}$ is a minimizer of (43). This completes the proof of Theorem 19. □

## 6. Convergence Analysis

In this section, we demonstrate that the solution of the minimization problem converges to the unique solution of the inverse problem being investigated as the regularization parameter tends to zero. We begin firstly by introducing the following concept of data compatibility:

**Definition 20.** *A function $\phi\in L^2(0,T;L^2(\partial\Omega))$ is said to be compatible data if the considered inverse source problem* (1)-(3) *admits a solution.*

**Theorem 21.** *Let $\phi\in L^2(0,T;L^2(\partial\Omega))$ be given compatible data and let $f^*=\chi_{\mathcal{D}^*}\in\mathcal{A}(\Omega)$ be a solution of the inverse source problem corresponding to the datum $\phi$. For any $\varrho>0$, let $\phi_\varrho\in L^2(0,T;L^2(\partial\Omega))$ be a noisy data satisfying*

$$\Big|\Big|\phi_\varrho-\phi\Big|\Big|_{L^2(0,T;L^2(\partial\Omega))}\le\varrho, \tag{75}$$

*and let $\eta(\varrho)=o(1)$ and $\frac{\varrho^2}{\eta(\varrho)}$ is bounded as $\varrho\to 0$. Define $f_\varrho=\chi_{\mathcal{D}_\varrho}$ as a solution to the following shape optimization problem:*

$$\underset{f=\chi_{\mathcal{D}}\in\mathcal{A}(\Omega)}{\text{Minimize}}\ \mathcal{K}_{\eta(\varrho)}(f):=\int_0^T\int_\Omega\Big|u_2[f,\phi_\varrho]\Big|^2\,\mathrm{d}x\mathrm{d}t+\eta(\varrho)\,P_\Omega(\mathcal{D}), \tag{76}$$

*where $u_2[f,\phi_\varrho]$ is the imaginary part of $\boldsymbol{u}[f,\phi_\varrho]$. Here, $\boldsymbol{u}[f,\phi_\varrho]=u_1[f,\phi_\varrho]+\boldsymbol{i}\,u_2[f,\phi_\varrho]$ is the solution of (66) with $\phi_\varrho$ replacing $\phi_n$. Then, as $\varrho\longrightarrow 0$, we have $\mathcal{D}\varrho\longrightarrow\mathcal{D}^*$ in the sense of characteristic functions.*

*Proof.* For each $\varrho$, we denote by $f_\varrho=\chi_{\mathcal{D}_\varrho}$ the solution to the regularized optimization problem (76). Let us consider the solution $f^*=\chi_{\mathcal{D}^*}$ to the inverse source problem corresponding to the measured Neumann data $\phi$. Since $f_\varrho=\chi_{\mathcal{D}_\varrho}$ is a minimizer of the minimization problem (76), we have

$$\int_0^T\int_\Omega\Big|u_2[f_\varrho,\phi_\varrho]\Big|^2\mathrm{d}x\mathrm{d}t+\eta(\varrho)\,P_\Omega(\mathcal{D}_\varrho)\leq\int_0^T\int_\Omega\Big|u_2[f^*,\phi_\varrho]\Big|^2\mathrm{d}x\mathrm{d}t+\eta(\varrho)\,P_\Omega(\mathcal{D}^*).$$

In addition, we have

$$\begin{aligned}\int_0^T\int_\Omega\Big|u_2[f^*,\phi_\varrho]\Big|^2\mathrm{d}x\mathrm{d}t&\leq 2\Big(\int_0^T\int_\Omega\Big|u_2[f^*,\phi_\varrho]-u_2[f^*,\phi]\Big|^2\mathrm{d}x\mathrm{d}t+\int_0^T\int_\Omega\Big|u_2[f^*,\phi]\Big|^2\mathrm{d}x\mathrm{d}t\Big)\\&\leq 2\Big(\Big|\Big|\Big|\boldsymbol{u}[f^*,\phi_\varrho]-\boldsymbol{u}[f^*,\phi]\Big|\Big|\Big|^2_{\mathbf{B}^{\frac{\alpha}{2}}(\Omega)}+\Big|\Big|u_2[f^*,\phi]\Big|\Big|^2_{L^2(0,T;L^2(\Omega))}\Big).\end{aligned}$$

Using the fact that $f^*=\chi_{\mathcal{D}^*}$ is a solution of the inverse problem corresponding to the measured $\phi$, one can deduce that $u_2[f^*,\phi]=0$ in $(0,\,T)\times\Omega$. Hence,

$$\int_0^T\int_\Omega\Big|u_2[f^*,\phi_\varrho]\Big|^2\mathrm{d}x\mathrm{d}t\leq 2\Big|\Big|\Big|\boldsymbol{u}[f^*,\phi_\varrho]-\boldsymbol{u}[f^*,\phi]\Big|\Big|\Big|^2_{\mathbf{B}^{\frac{\alpha}{2}}(\Omega)}.\tag{77}$$

Consequently,

$$\int_0^T\int_\Omega\Big|u_2[f_\varrho,\phi_\varrho]\Big|^2\mathrm{d}x\mathrm{d}t+\eta(\varrho)\,P_\Omega(\mathcal{D}_\varrho)\leq 2\Big|\Big|\Big|\boldsymbol{u}[f^*,\phi_\varrho]-\boldsymbol{u}[f^*,\phi]\Big|\Big|\Big|^2_{\mathbf{B}^{\frac{\alpha}{2}}(\Omega)}+\eta(\varrho)\,P_\Omega(\mathcal{D}^*).\tag{78}$$

Let us now estimate the term $\Big|\Big|\Big|\boldsymbol{u}[f^*,\phi_\varrho]-\boldsymbol{u}[f^*,\phi]\Big|\Big|\Big|^2_{\mathbf{B}^{\frac{\alpha}{2}}(\Omega)}$. Consider the difference $\boldsymbol{w}_\varrho=\boldsymbol{u}[f^*,\phi_\varrho]-\boldsymbol{u}[f^*,\phi]$ which is the solution to

$$\left\{\begin{array}{rcll}\partial_t^\alpha\boldsymbol{w}_\varrho-\Delta\boldsymbol{w}_\varrho+\boldsymbol{w}_\varrho&=&0&\text{in}\quad(0,T)\times\Omega,\\ \partial_\nu\boldsymbol{w}_\varrho+\boldsymbol{i}\,\boldsymbol{w}_\varrho&=&\phi_\varrho-\phi&\text{on}\quad(0,T)\times\partial\Omega,\\ \boldsymbol{w}_\varrho(\cdot,0)&=&0&\text{in}\quad\Omega.\end{array}\right.\tag{79}$$

Again using the same technique described in the proof of (55), one can prove that

$$\Big|\Big|\Big|\boldsymbol{w}_\varrho\Big|\Big|\Big|^2_{\mathbf{B}^{\frac{\alpha}{2}}(\Omega)}=\Big|\Big|\Big|\boldsymbol{u}[f^*,\phi_\varrho]-\boldsymbol{u}[f^*,\phi]\Big|\Big|\Big|^2_{\mathbf{B}^{\frac{\alpha}{2}}(\Omega)}\leq C\Big|\Big|\phi_\varrho-\phi\Big|\Big|^2_{L^2(0,T;L^2(\partial\Omega))}.\tag{80}$$

Inserting (80) into (78) and using condition (75), one can conclude that

$$\int_0^T\int_\Omega\Big|u_2[f_\varrho,\phi_\varrho]\Big|^2\mathrm{d}x\mathrm{d}t+\eta(\varrho)P_\Omega(\mathcal{D}_\varrho)\leq\varrho^2+\eta(\varrho)\,P_\Omega(\mathcal{D}^*)\longrightarrow 0\ \text{ as }\ \varrho\longrightarrow 0.\tag{81}$$

Therefore, we have

$$P_\Omega(\mathcal{D}_\varrho)\leq\frac{\varrho^2}{\eta(\varrho)}+\,P_\Omega(\mathcal{D}^*)\leq C.$$

Consequently, in view of [24, Theorem 6.3 in Chapter 5], we can extract a subsequence of $\{f_\varrho=\chi_{\mathcal{D}_\varrho}\}_\varrho$ (which we denote by $\{f_\varrho=\chi_{\mathcal{D}_\varrho}\}_\varrho$ for simplicity) such that

$$f_\varrho=\chi_{\mathcal{D}_\varrho}\longrightarrow f^0=\chi_{\mathcal{D}^0}\ \text{ in }\ L^1(\Omega)\ \text{ as }\ \varrho\longrightarrow 0,\tag{82}$$

for some $f^0=\chi_{\mathcal{D}^0}\in\mathcal{A}(\Omega)$. On the other hand, we have

$$\int_0^T\int_\Omega\Big|u_2[f^0,\phi]\Big|^2\mathrm{d}x\mathrm{d}t\leq 2\int_0^T\int_\Omega\Big|u_2[f^0,\phi]-u_2[f_\varrho,\phi_\varrho]\Big|^2\mathrm{d}x\mathrm{d}t+2\int_0^T\int_\Omega\Big|u_2[f_\varrho,\phi_\varrho]\Big|^2\mathrm{d}x\mathrm{d}t.\tag{83}$$

Again by the same analysis as in the proof of (72), we can derive

$$u_2[f^0, \phi] - u_2[f_\varrho, \phi_\varrho] \longrightarrow 0 \quad \text{in} \quad L^2(0, T; L^2(\Omega)) \ \text{ as } \ \varrho \longrightarrow 0.$$

Using (81) and from the last relation, we get

$$u_2[f^0, \phi] = 0 \ \text{ in } \ (0,\, T) \times \Omega,$$

which implies that $f^0$ is a solution of the inverse problem and by the uniqueness of the inverse problem (see Theorem 9) we can deduce $f^0 = f^*$. This achieves the proof. □

## 7. Sensitivity analysis

The geometric inverse source problem under consideration has been reformulated as a topology optimization problem (43). To address this, we present an approach based on the topological derivative method. In order to provide a complete understanding of the methodology, we briefly introduce the fundamental concept of the topological gradient and discuss the crucial regularization issue presented in this paper, which is described in Section 7.1. Then, in Section 7.2, we derive a second-order topological asymptotic expansion of the shape functional considered in this study.

### 7.1. Topological gradient-based reconstruction: regularization and robustness.

In this paper, we propose a fast and accurate reconstruction approach based on the topological sensitivity to solve the topology optimization problem (43). The concept of topological sensitivity (or topological derivative) was introduced in [28, 71] and further developed in the book by Novotny and Sokołowski [64]. It belongs to a broader class of asymptotic methods, as discussed in the books by Della Riva et al. [21] and Ammari et al. [6, 8], for instance. The main idea of this concept is to measure the sensitivity of a given shape function to small topological perturbations in the domain, such as the creation of cavities, cracks, inclusions, or source terms.

Studying the topological derivative of $\mathcal{K}_\eta$ presents a significant challenge due to the presence of a penalization term, which is not a topological differential. Let us now address the crucial regularization issue that arises in this context. The topological gradient, particularly for $L^2$-norm misfit functions (or $H^1$-seminorm) without a regularization term, has been successfully utilized in inverse problems such as crack detection [9], obstacle localization [16, 15], reconstruction of small cavities in Stokes flow [1], detection of point-force locations in Stokes flows [26], and identification of source terms [12]. The advantage of topological gradient-based procedures is that they provide a non-iterative (or iterative) reconstruction algorithm, which requires only a minimal number of user-defined algorithmic parameters and is free of an initial guess, in contrast to traditional optimization procedures. In the latter, many parameters, such as the initial guess, regularization parameter, step size, etc., must be carefully chosen to enhance the stability of the numerical procedure and ensure the optimization process (see, for example, [68, 37]). Moreover, numerical simulations in the literature have shown that topological gradient-based procedures are highly robust with respect to noisy data. For instance, in the context of gravimetry, Menoret, Hrizi, and Novotny [61] discussed the robustness of the topological gradient method using four different error norms (without a regularization term), namely, the $H^1(\Omega)$-norm, $H^1(\Omega)$-seminorm, $L^2(\Omega)$-norm, and $L^2(\Gamma_M)$-norm, where $\Gamma_M \subset \partial\Omega$. They proved that the $L^2(\Omega)$-norms, which are the focus of our work, are more robust with respect to noise in numerical simulations. Despite the extensive investigation of the topological derivative method, the theoretical aspect of the robustness issue has not been addressed so far.

Based on the discussion above, one can conclude that the topological derivative method provides a fast and accurate numerical optimization algorithm, which means that no additional regularization term is needed to stabilize the reconstruction process. Thus, for the sake of simplicity, we disregard the impact of the regularization term in (42) by setting the penalization term to zero. In fact, we assume that $P_\Omega(\mathcal{D}) < +\infty$ and choose $\eta = 0$. To this end, we will

define the functional $\mathcal{K}_\eta$ in the following way throughout the rest of the paper:

$$\mathcal{K}(f) = \int_0^T \int_\Omega \Big| u_2[f] \Big|^2 \mathrm{d}x\mathrm{d}t \ \text{ for all } \ f \in \mathcal{A}(\Omega). \tag{84}$$

7.2. **Asymptotic analysis.** To derive a second-order topological asymptotic expansion for $\mathcal{K}$ in the presence of a finite number of ball-shaped sources, we must introduce some notation.

Let $m \geq 1$ be a given integer. For each $1 \leq j \leq m$, we denote by $\mathcal{B}_{\varepsilon_j}(s_j)$ the ball of radius $\varepsilon_j$ centered at $s_j \in \Omega$. We assume that the balls $\mathcal{B}_{\varepsilon_j}(s_j)$ are disjoint and strictly contained within the domain $\Omega$, i.e., $\overline{\mathcal{B}_{\varepsilon_j}(s_j)} \subset \Omega$, and $\mathcal{B}_{\varepsilon_j}(s_j) \cap \mathcal{B}_{\varepsilon_k}(s_k) = \emptyset$ for all $j, k \in \{1, \cdots, m\}$ with $j \neq k$.

Let us recall that the source term for the complex time-fractional diffusion problems (38) is given by

$$F(t,x) = \zeta(t)\, \chi_{\mathcal{D}}(x),$$

where $\zeta$ and $\chi_{\mathcal{D}}$ represent the time-dependent function in $L^2(0,\, T)$ and characteristic function of the spatial domain $\mathcal{D}$, respectively. On the other hand, since $\zeta(t)$ is known, for the sake of completeness, we assume that it is given in the form of a piecewise function, where each component $\zeta_i$ is associated with the ball $\mathcal{B}_{\varepsilon_j}(s_j)$ for $j = 1, \cdots, m$. From this, we can define the perturbed counterpart of the source term $F$ as follows

$$F^\varepsilon(t,x) = \zeta(t)\, f(x) + \sum_{j=1}^m \sigma_j \chi_{\mathcal{B}_{\varepsilon_j}(s_j)}(x), \tag{85}$$

where $f = \chi_{\mathcal{D}}$ and $\sigma_j \in \mathbb{R}^+$ is associated with the mean value of $\zeta_j(t)$, namely

$$\sigma_j = \frac{1}{T} \int_0^T \zeta_j(t) \mathrm{d}t. \tag{86}$$

Based on this, we define the shape functional associated with the topologically perturbed source term (85) as

$$\mathcal{K}(F^\varepsilon) = \int_0^T \int_\Omega \Big| u_2^\varepsilon \Big|^2 \mathrm{d}x\mathrm{d}t \tag{87}$$

where $\boldsymbol{u}^\varepsilon = u_1^\varepsilon + \boldsymbol{i}\, u_2^\varepsilon$ is solution of the perturbed complex boundary value problem of the form

$$\left\{ \begin{array}{rcll} \partial_t^\alpha \boldsymbol{u}^\varepsilon - \Delta \boldsymbol{u}^\varepsilon + \boldsymbol{u}^\varepsilon &=& F^\varepsilon & \text{in} \quad (0,T) \times \Omega, \\ \partial_\nu \boldsymbol{u}^\varepsilon + \beta \boldsymbol{i}\, \boldsymbol{u}^\varepsilon &=& \phi + \beta \boldsymbol{i}\, \varphi & \text{on} \quad (0,T) \times \partial\Omega, \\ \boldsymbol{u}^\varepsilon(.,0) &=& \xi^\varepsilon & \text{in} \quad \Omega. \end{array} \right. \tag{88}$$

We will use these elements to derive an asymptotic formula that describes the variation of $\mathcal{K}(F^\varepsilon) - \mathcal{K}(f)$ with respect to $\varepsilon$. Subsequently, we introduce the following ansatz for the solution to the perturbed problem (88):

$$\boldsymbol{u}^\varepsilon(t,x) = \boldsymbol{u}[f](t,x) + \sum_{j=1}^n \sigma_j \pi \varepsilon_j^2 \boldsymbol{v}^{\varepsilon_j}(x), \tag{89}$$

where $\boldsymbol{u}[f] = u_1[f] + \boldsymbol{i}\, u_2[f]$ solves the complex boundary value problem (38) and $\boldsymbol{v}^{\varepsilon_j} = v_1^{\varepsilon_j} + \boldsymbol{i}\, v_2^{\varepsilon_j}$ is the solution of the following auxiliary boundary value problem for $j = 1, \cdots, n$:

$$\left\{ \begin{array}{rcll} -\Delta \boldsymbol{v}^{\varepsilon_j} + \boldsymbol{v}^{\varepsilon_j} &=& \frac{1}{\pi \varepsilon_j^2} \chi_{\mathcal{B}_{\varepsilon_j}(s_j)} & \text{in} \quad \Omega, \\ \partial_\nu \boldsymbol{v}^{\varepsilon_j} + \beta \boldsymbol{i}\, \boldsymbol{v}^{\varepsilon_j} &=& 0 & \text{on} \quad \partial\Omega. \end{array} \right. \tag{90}$$

The ansatz (89) leads to an initial condition of the form $\xi^\varepsilon(x) = \sum_{j=1}^m \sigma_j \pi \varepsilon_j^2 \boldsymbol{v}^{\varepsilon_j}(x)$ for the perturbed complex boundary value problem (88).

Now, let us decompose $\boldsymbol{v}^{\varepsilon_j}$, solution of (90), into two parts as follows

$$\boldsymbol{v}^{\varepsilon_j}(x) = p^{\varepsilon_j}(x) + \lambda_3^{\varepsilon_j} \boldsymbol{q}^j(x), \tag{91}$$

where $p^{\varepsilon_j}$ is the solution to the following boundary value problem (92), defined in a large ball $\mathcal{B}_R(s_j)$ with radius $R$ and center at $s_j$, which contains $\Omega$ (i.e. $\Omega \subset \mathcal{B}_R(s_j)$)

$$\left\{ \begin{array}{rcll} -\Delta p^{\varepsilon_j} + p^{\varepsilon_j} & = & \frac{1}{\pi\varepsilon_j^2}\chi_{\mathcal{B}_{\varepsilon_j}(s_j)} & \text{in} \quad \mathcal{B}_R(s_j), \\ p^{\varepsilon_j} & = & \lambda_3^{\varepsilon_j} K_0(R) & \text{on} \quad \partial\mathcal{B}_R(s_j). \end{array} \right. \tag{92}$$

Problem (92) can be solved analytically and its solution is

$$p^{\varepsilon_j}(x) = \left\{ \begin{array}{ll} \lambda_3^{\varepsilon_j} K_0(\|x - s_j\|) & x \in \mathcal{B}_R(s_j) \setminus \overline{\mathcal{B}_{\varepsilon_j}(s_j)}, \\ \lambda_1^{\varepsilon_j} - \lambda_2^{\varepsilon_j} I_0(\|x - s_j\|) & x \in \mathcal{B}_{\varepsilon_j}(s_j), \end{array} \right. \tag{93}$$

where

$$\lambda_1^{\varepsilon_j} = \frac{1}{\pi\varepsilon_j^2}, \quad \lambda_2^{\varepsilon_j} = \frac{1}{\pi\varepsilon_j^2} \frac{K_1(\varepsilon_j)}{I_0(\varepsilon_j)K_1(\varepsilon_j) + I_1(\varepsilon_j)K_0(\varepsilon_j)}, \tag{94}$$

and

$$\lambda_3^{\varepsilon_j} = \frac{1}{\pi\varepsilon_j^2} \frac{I_1(\varepsilon_j)}{I_0(\varepsilon_j)K_1(\varepsilon_j) + I_1(\varepsilon_j)K_0(\varepsilon_j)} \tag{95}$$

with the modified Bessel functions $I_0$, $I_1$, $K_0$, and $K_1$ given in the Appendix A through equations (108), (109), (110) and (111), respectively.

Finally, $\lambda_3^{\varepsilon_j}\boldsymbol{q}^j$ must compensate for the discrepancies left by $p^{\varepsilon_j}$ on $\partial\Omega$. Specifically, $\boldsymbol{q}^j = q_1^j + \boldsymbol{i}\, q_2^j$ is the solution to the following boundary value problem

$$\left\{ \begin{array}{rcll} -\Delta \boldsymbol{q}^j + \boldsymbol{q}^j & = & 0 & \text{in } \Omega, \\ \partial_\nu \boldsymbol{q}^j + \beta \boldsymbol{i}\, \boldsymbol{q}^j & = & -\partial_\nu K_0(\|x - s_j\|) - \beta \boldsymbol{i}\, K_0(\|x - s_j\|) & \text{on } \partial\Omega. \end{array} \right.$$

Consequently, from (89), we have the following expansion:

$$\begin{aligned} u_2^\varepsilon(t,x) = \mathfrak{I}\Big\{\boldsymbol{u}^\varepsilon(t,x)\Big\} &= \mathfrak{I}\Big\{\boldsymbol{u}[f](t,x)\Big\} + \sum_{j=1}^n \lambda^{\varepsilon_j} \mathfrak{I}\Big\{\boldsymbol{q}^j(x)\Big\} \\ &= u_2[f](t,x) + \sum_{j=1}^n \lambda^{\varepsilon_j} q_2^j(x) \quad \text{for all } (t,x) \in (0,T)\times\Omega. \end{aligned} \tag{96}$$

with $\lambda^{\varepsilon_j}$ given by

$$\lambda^{\varepsilon_j} = \sigma_j \frac{I_1(\varepsilon_j)}{I_0(\varepsilon_j)K_1(\varepsilon_j) + I_1(\varepsilon_j)K_0(\varepsilon_j)}. \tag{97}$$

By substituting (96) into (87), we obtain the following asymptotic expansion:

$$\mathcal{K}(F^\varepsilon) - \mathcal{K}(f) = 2\sum_{j=1}^m \lambda^{\varepsilon_j} \int_\Omega q_2^j \left( \int_0^T u_2[f]\, \mathrm{d}t \right) \mathrm{d}x + T \sum_{j,k=1}^m \lambda^{\varepsilon_j}\lambda^{\varepsilon_k} \int_\Omega q_2^j q_2^k \, \mathrm{d}x. \tag{98}$$

The above topological asymptotic expansion can be rewritten in the following compact form

$$\mathcal{K}(F^\varepsilon) = \mathcal{K}(f) + \Phi_m(\lambda, s).$$

The quantity $\Phi_m(\lambda, s)$ is defined as

$$\Phi_m(\lambda, s) = \lambda \cdot d(s) + \frac{1}{2} H(s)\lambda \cdot \lambda, \tag{99}$$

where vectors $s = (s_1, \cdots, s_m)$ and $\lambda = (\lambda_1, \cdots \lambda_m)$, with $\lambda_j = \lambda^{\varepsilon_j}$. Moreover, $d(s)$ and $H(s)$ are the first and second order topological derivatives, respectively. The vector $d$ and matrix $H$ have entries

$$d = \begin{pmatrix} d_1 \\ d_2 \\ \vdots \\ d_m \end{pmatrix} \quad \text{and} \quad H = \begin{pmatrix} H_{11} & H_{12} & \cdots & H_{1m} \\ H_{21} & H_{22} & \cdots & H_{2m} \\ \vdots & \vdots & \ddots & \vdots \\ H_{m1} & H_{m2} & \cdots & H_{mm} \end{pmatrix}, \tag{100}$$

where

$$d_j = 2\int_\Omega q_2^j \left(\int_0^T u_2[f]\,\mathrm{d}t\right)\mathrm{d}x \quad \text{and} \quad H_{jk} = 2T\int_\Omega q_2^j q_2^k\,\mathrm{d}x. \tag{101}$$

Given the general function of form (99), the minimum is found when:

$$\langle D_\lambda \Phi_m(\lambda, s), \mu\rangle = 0 \quad \forall \mu \in \mathbb{R}^m. \tag{102}$$

Furthermore, since $H$ is a symmetric and positive definite matrix, the minimum of the function with respect to $\lambda$ is the global optimum. In particular,

$$(H(s)\lambda + d(s)) \cdot \mu = 0 \quad \forall \mu \in \mathbb{R}^m \quad \Rightarrow \quad H(s)\lambda = -d(s), \tag{103}$$

provided that $H = H^\top$. Therefore,

$$\lambda = \lambda(s) = -H(s)^{-1}d(s), \tag{104}$$

such that the quantity $\lambda$, solving (104), becomes a function of the locations $s$. Substituting the solution of (104) into $\Phi_m(\lambda, s)$, defined by (99), the optimal locations $s^\star$ can be obtained from a combinatorial search over the domain $\Omega$. These locations are the solutions to the following minimization problem:

$$s^\star = \underset{s\subset S}{\operatorname{argmin}} \left\{ \Phi_m(\lambda(s), s) = \frac{1}{2}\lambda(s)\cdot d(s) \right\}, \tag{105}$$

where $S$ is the set of admissible source locations. Then, the optimal sources are characterized by $\lambda^\star = \lambda(s^\star)$. Finally, each unknown $\lambda_j = \lambda^{\varepsilon_j}$ from (97) can be written as an expansion with respect to $\varepsilon_j$ as follows:

$$\lambda^{\varepsilon_j} = \frac{\sigma_j \pi \varepsilon_j^2}{2\pi} + O(\varepsilon_j^4). \tag{106}$$

Therefore, the volume of the $j$-th source can be approximated by $\sigma_j\pi\varepsilon_j^2 \approx 2\pi\lambda_j$, where $\sigma_j$ is given by (86). For more details on the resulting reconstruction algorithm, the reader may refer to [61], for instance.

## 8. Numerical reconstruction

We consider a square-shaped domain $\Omega = (0,1)\times(0,1)$. The boundary value problems are discretized by using standard Finite Element Method in space and Finite Difference Method in time following the same procedure as described in [68]. In particular, the domain $\Omega$ is discretized into 102400 three-node finite elements. The set of admissible locations $S$ is obtained by selecting 181 interior nodes from the finite elements mesh. See sketch in Figure 1, where the points belonging to $S$ are represented by black dots. Finally, the final time is set as $T = 1$ and the resulting interval $(0,1)$ is discretized into 100 uniform time steps.

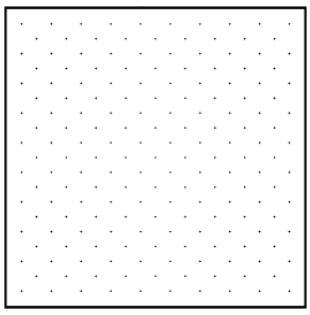

Figure 1. Domain $\Omega$ and set of admissible locations $S$ represented by 181 black dots.

We note that, once the location of the true source does not belong to the set of admissible locations $S$, the reconstruction algorithm returns the optimal location closest to the true one.

See for instance the original work [12]. Thus, for the sake of simplicity, we assume that the true locations of sources to be reconstructed always belongs to the set $S$.

The source $F^*(t,x)$ to be reconstructed is given by

$$F^*(t,x) = \sum_{i=1}^{m} \zeta_i(t)\chi_{\mathcal{D}_i^*}(x), \tag{107}$$

where $m$ is the number of hidden sources and $\mathcal{D}_i^*$, for $i = 1, \cdots, m$, are their geometrical supports, with $\mathcal{D}_i^* \cap \mathcal{D}_j^* = \varnothing$, for $i \neq j$. The mean values of functions $\zeta_i(t)$ are set as $\sigma_i = 1$, for $i = 1, \cdots, m$. This choice simplifies the graphical representation of the results, since each unknown $\lambda_i$ is proportional to the volume of the $i$-th source through expansion (106).

Note that the number of sources $m$ to be reconstructed is arbitrary. However, for the sake of simplicity, we assume that $m$ is given. In the case of unknown $m$, see for instance [12]. In addition, we set $\beta = 10$ and $\varphi = 0$ in all examples. Finally, we set $f(x) = 0$ (i.e., $\mathcal{D} = \varnothing$), for all $x \in \Omega$, which means that all the examples are free of initial guess. The choice $\beta = 10$ is explained in details through Example 4 in Section 8.4.

8.1. **Example 1.** In this example, we consider the reconstruction of a circular-shaped source of radius 0.05, as shown in Figure 2. The function $\zeta_1(t)$ is given by

$$\zeta_1(t) = 10, \text{ for } 0 < t \leq 0.1, \text{ and } \zeta_1(t) = 0, \text{ otherwise.}$$

Therefore, $\sigma_1 = 1$ by construction. The obtained results by setting $\alpha = \{0.1, 0.5, 0.9\}$ are presented in Figure 3. From an analysis of these figures, we observe that the reconstruction is nearly exact independent of $\alpha$, so that in the next examples we fix $\alpha = 0.5$. For the sake of completeness, the quantitative results are reported in Table 1.

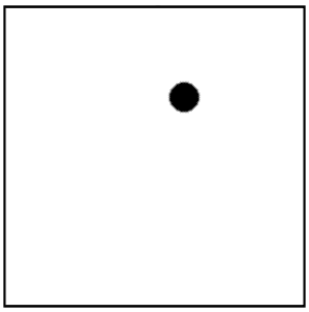

FIGURE 2. Example 1: Target to be reconstructed.

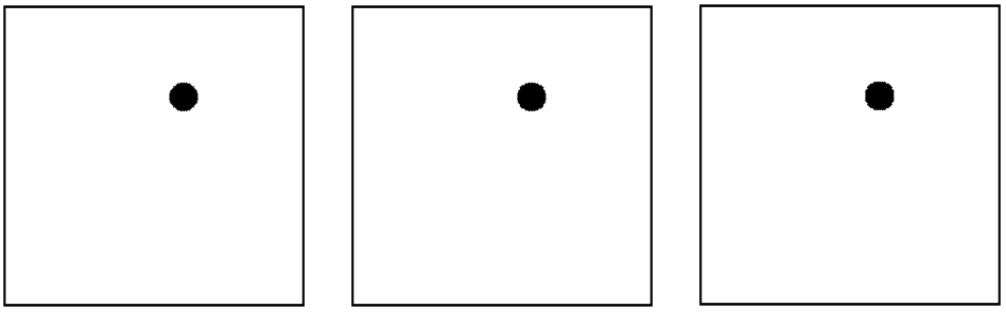

(a) $\alpha = 0.1$ (b) $\alpha = 0.5$ (c) $\alpha = 0.9$

FIGURE 3. Example 1: Obtained results for varying values of $\alpha$.

TABLE 1. Example 1: Quantitative summary of the obtained results.

| $\alpha$ | 0.1 | 0.5 | 0.9 |
|---|---|---|---|
| radius | 0.0487 | 0.0491 | 0.0497 |

8.2. **Example 2.** Now, let us consider the simultaneous reconstruction of two circular-shaped sources of radii 0.05 and 0.1, as shown in Figure 4(a). The functions $\zeta_1(t)$ and $\zeta_2(t)$ are respectively given by

$$\zeta_1(t) = 10, \text{ for } 0 < t \leq 0.1 \text{ and } \zeta_1(t) = 0, \text{ otherwise;}$$

$$\zeta_2(t) = 5, \text{ for } 0.2 < t \leq 0.4 \text{ and } \zeta_2(t) = 0, \text{ otherwise.}$$

In this way, $\sigma_1 = \sigma_2 = 1$. The obtained result for $\alpha = 0.5$ is presented in Figure 4(b). Once again, the reconstruction is nearly exact.

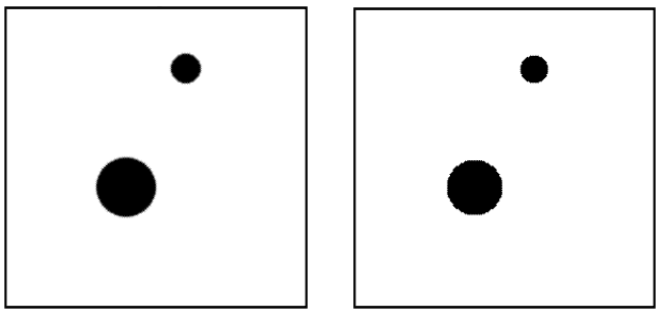

(a) target (b) result

FIGURE 4. Example 2: Target to be reconstructed (a) and obtained reconstruction (b).

8.3. **Example 3.** Now, let us consider the simultaneous reconstruction of three identical circular-shaped sources with radii 0.05, as shown in Figure 5(a). The functions $\zeta_1(t)$, $\zeta_2(t)$ and $\zeta_3(t)$ are also identical and given by

$$\zeta_i(t) = 10, \text{ for } 0 < t \leq 0.1 \text{ and } \zeta_i(t) = 0, \text{ otherwise; for } i = 1, 2, 3.$$

Therefore, $\sigma_1 = \sigma_2 = \sigma_3 = 1$. The obtained result for $\alpha = 0.5$ is reported in Figure 5(b), showing a nearly exact reconstruction, as expected.

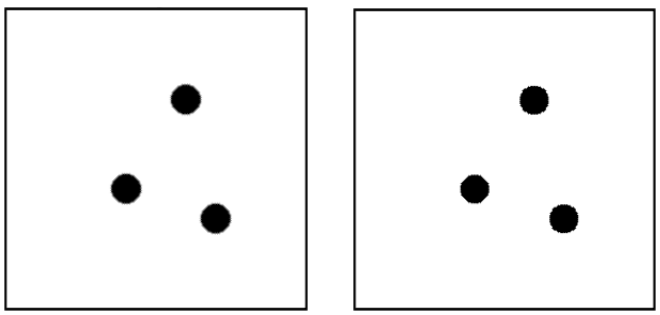

(a) target (b) result

FIGURE 5. Example 3: Target to be reconstructed (a) and obtained reconstruction (b) with $m = 3$ trial balls.

8.4. **Example 4.** In this example, the idea is to reconstruct an L-shaped source, as presented in Figure 6, by setting $m = 3$ trial balls. The function $\zeta_1(t)$ is given by

$$\zeta_1(t) = 10, \text{ for } 0 < t \leq 0.1, \text{ and } \zeta_1(t) = 0, \text{ otherwise.}$$

Therefore, $\sigma_1 = 1$. The obtained results for various values of $\beta$, namely $\beta \in \{1, 2, 3, 8\}$, are presented in Figure 7. We note that for $\beta \in \{1, 2\}$, the reconstruction is far from the L-shaped target. However, after increasing it up to $\beta \in \{4, 8\}$, the solution becomes stable and close to the target. In particular, after setting $\beta = 10$, we observe that the L-shaped source can be quite well approximated by the three trial balls, as can be seen in Figure 8.

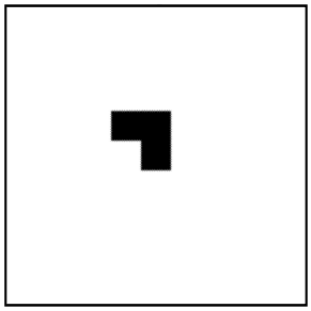

FIGURE 6. Example 4: Target to be reconstructed.

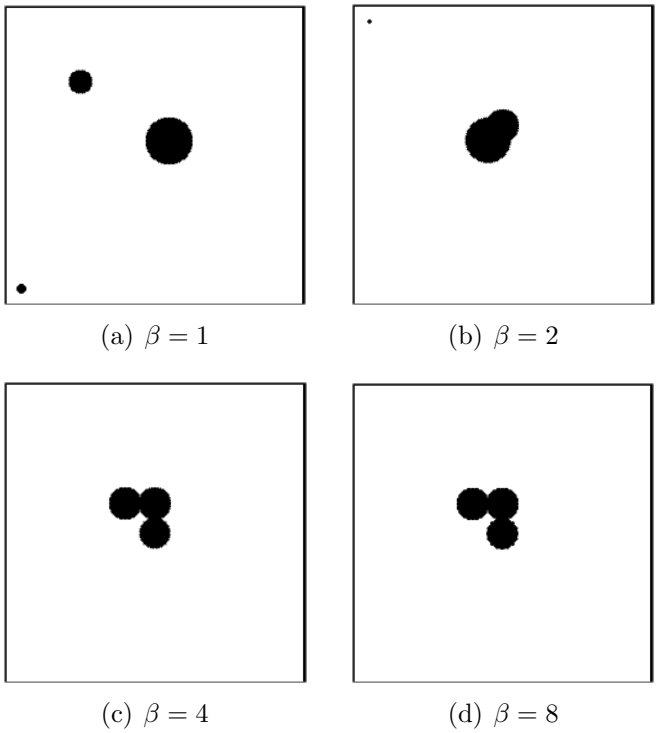

(a) $\beta = 1$ (b) $\beta = 2$

(c) $\beta = 4$ (d) $\beta = 8$

FIGURE 7. Example 4: Obtained reconstructions for varying values of $\beta$ and $m = 3$ trial balls.

8.5. **Example 5.** Finally, in order to verify the robustness of the reconstruction algorithm with respect to noisy data, the true source term $F(t, x)$ is corrupted with White Gaussian Noise (WGN) of zero mean. Note that, in this context, noisy data can be interpreted as modelling uncertainties. In particular, we consider the reconstruction of a cross-shaped source by setting $m = 1$ trial ball. The target is corrupted with varying levels of noise, namely $\{40, 80, 120\}\%$ as shown in Figure 9, left column. The obtained results are presented in Figure 9, right column.

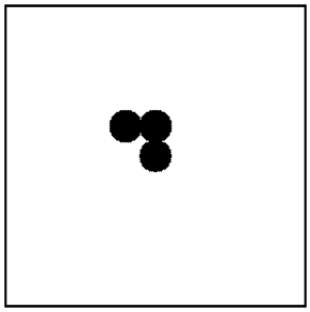

FIGURE 8. Example 4: Obtained reconstruction for $\beta = 10$ and $m = 3$ trial balls.

From an analysis of these figures, we observe that the center of the trial ball coincides with the barycenter of the cross-shaped source and the resulting volumes are very close to each other, up to 80% of noise. For 120% of noise, the center of the reconstructed source gets lost and the volume is slight underestimated. It shows that a trial ball can be used to approximate the cross-shaped source even in the presence of high level of noisy data.

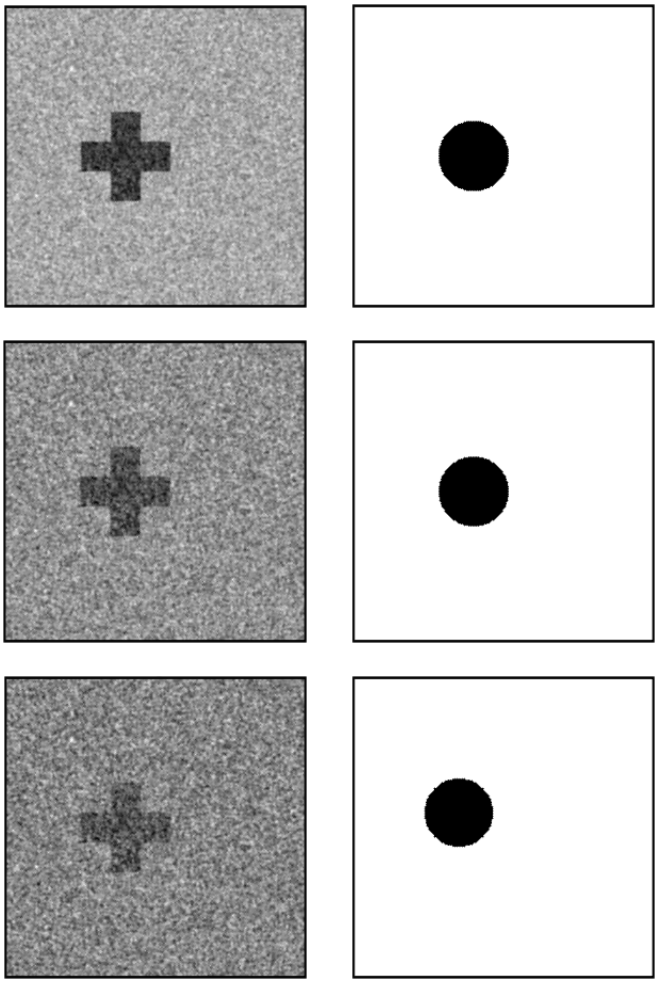

FIGURE 9. Example 5: Target to be reconstructed (left column) and obtained reconstructions with $m = 1$ trial ball (right column). The level of noise is increased from the first to the third line as $\{40, 80, 120\}\%$, respectively.

Let us conclude the numerical experiments with a comparison between the coupled complex boundary method (CCBM) and the Kohn-Vogelius (KV) approach from [65]. We introduce the

errors in the volume and in the barycenter as follows

$$\mathcal{E}_V = \frac{|V^* - V^\star|}{V^*} \qquad \text{and} \qquad \mathcal{E}_S = \frac{\|s^* - s^\star\|}{\|s^*\|},$$

where $(V^*, s^*)$ and $(V^\star, s^\star)$ are the volume and barycenter of the target and the reconstructed shapes, respectively. The total error $\mathcal{E}_T = \mathcal{E}_V + \mathcal{E}_S$ are reported in Table 2 for several level of noise. From an analysis of the obtained results, we observe that CCBM and KV are equivalent in terms of resilience with respect to noisy data, with a slight superiority of CCBM for the test case in particular.

TABLE 2. Example 5. Error $\mathcal{E}_T$ (%) for varying level of noise (%).

| noise level | CCBM | KV |
|---|---|---|
| 0 | 3.66 | 4.58 |
| 40 | 4.33 | 5.62 |
| 80 | 5.00 | 6.66 |
| 120 | 12.13 | 11.04 |

## 9. Further comments and conclusions

In this paper, we proposed a novel approach, called the Complex Coupled Boundary Method (CCBM), to solve a geometric inverse source problem governed by the two-dimensional time-fractional diffusion equation. The CCBM method is based on a straightforward concept: the coupling of Dirichlet and Neumann data through a Robin boundary condition. This is achieved by defining the Robin boundary condition in a way that the Dirichlet and Neumann data correspond to its respective real and imaginary parts. By doing so, the conditions that must be satisfied on the accessible boundary are transformed into a single condition that needs to be fulfilled on the domain itself.

From this idea, the inverse source problem is reformulated as an optimization problem that aims to fit the imaginary part of the solution to the complex boundary problem using a least-squares approach. Specifically, the unknown support of the space-dependent source is characterized as the solution to a self-regularized topology optimization problem minimizing the least-squares functional, with respect to the set of admissible sources, by using the topological derivative method.

We have established the existence, stability, and regularization properties of the solution for the optimization problem. Furthermore, we have demonstrated the uniqueness of the inverse source problem. Additionally, the second-order topological derivative has been exploited for devising a non-iterative reconstruction algorithm, which is free of initial guess, in the sense that $\mathcal{D} = \varnothing$ ($f = 0$), and very robust with respect to noisy data. As for the crucial regularization issue, the topological derivative method for tracking-type functional has repeatedly been noticed to be self-regularizing, which means they don't need an additional regularization to stabilize the detection process. However, it is important to mathematically prove this feature in the present case.

From a theoretical standpoint, computing the second-order topological derivative of the cost function $\mathcal{K}$ is simpler using the CCBM approach than the Kohn-Vogelius functional $\mathcal{J}$ from (5) (see [65]). This is because the topological derivative expression for CCBM involves only one equality constraint (corresponding to problem (38)), in addition to the objective function $\mathcal{K}$. In contrast, the Kohn-Vogelius formulation requires two equality constraints corresponding to a Neumann problem and a Dirichlet problem. From a numerical perspective, the CCBM and Kohn-Vogelius methods are comparable in terms of computational cost and robustness to noise. However, in the test case presented, the CCBM method shows a slight advantage. Additionally, the proposed reconstruction algorithm for CCBM involves solving just one set of complex boundary value problems, whereas the Kohn-Vogelius method requires solving two

sets of boundary value problems, where each set has a number card($S$) of BVPs to be solved (card($S$) = 181 in the numerical examples from Section 8).

A direct numerical comparison between CCBM and the methods of Rundell and Zhang [68] and Hu and Zhu [36] is not feasible, as each method is built upon fundamentally different strategies. Nonetheless, the following key distinctions can be noted:

- The methods in [36, 68] are iterative, whereas our proposed approach is non-iterative.
- Our method does not require an initial guess, unlike the approache in [36], which rely heavily on the choice of the initial guess.
- Since the proposed method can accurately approximate the unknown support source using multiple small balls, it can serve as an effective initial guess for other iterative methods such as those studied in [36].

This article mainly focuses on topological sensitivity analysis and certain algorithmic aspects, and hence, several important mathematical issues remain unaddressed. One such issue is the stability of the inverse problem. To the best of our knowledge, the question of stability–either Lipschitz or logarithmic–remains open and deserves further investigation. Moreover, while the use of $L^2$-norm or $H^1$-seminorm misfit functionals has often been observed, and in some cases even proven, to act as a form of self-regularization (see, for example, [1, 13, 16, 35]), this property still requires a rigorous mathematical justification in the context of the present work. It is also worth noting that the theoretical stability of first-order topological derivative methods has been studied in the literature, notably by Ammari et al. [5, 7]. In particular, they demonstrated that imaging functionals based on topological derivatives exhibit enhanced robustness with respect to both measurement noise and medium perturbations, in comparison with more classical imaging approaches.

## Appendix A. Series expansions for Bessel functions

In this appendix, we provide the series expansions for modified Bessel functions of the first and second kind, denoted by $I_\ell$ and $K_\ell$, respectively. The order of these functions is denoted by $\ell \in \mathbb{Z}$, and the expansions are valid as $r \to 0^+$.

The modified Bessel function of the first kind and order $\ell$, $I_\ell$, has the following asymptotic expansions:

$$I_0(r) = 1 + \frac{1}{4}r^2 + \tilde{I}_0(r), \qquad \tilde{I}_0(r) = O(r^4) \tag{108}$$

and

$$I_1(r) = \frac{1}{2}r + \frac{1}{16}r^3 + \tilde{I}_1(r), \qquad \tilde{I}_1(r) = O(r^5). \tag{109}$$

The modified Bessel function of the second kind and order $\ell$, $K_\ell$, has the following asymptotic expansions:

$$K_0(r) = (\ln 2 - \mathrm{e}) - \ln r - \frac{1}{4}r^2 \ln r + \frac{1}{4}(1 + \ln 2 - \mathrm{e})r^2 + \tilde{K}_0(r), \quad \tilde{K}_0(r) = O(r^4) \tag{110}$$

and

$$K_1(r) = \frac{1}{r} + \frac{1}{2}r \ln r + \frac{1}{2}(\mathrm{e} - \ln 2 - \frac{1}{2})r + \frac{1}{16}r^3 \ln r + \frac{1}{16}(\mathrm{e} - \ln 2 - \frac{5}{4})r^3 + \tilde{K}_1(r), \quad \tilde{K}_1(r) = O(r^5), \tag{111}$$

where e is the Euler number. These series expansions were obtained from Jeffrey and Dai [38].

## Acknowledgements

This research was supported in part by CNPq (Brazilian Research Council), CAPES (Brazilian Higher Education Staff Training Agency) and FAPERJ (Research Foundation of the State of Rio de Janeiro).

## References


[1] A. B. Abda, M. Hassine, M. Jaoua, and M. Masmoudi. Topological sensitivity analysis for the location of small cavities in stokes flow. *SIAM Journal on Control and Optimization*, 48:2871–2900, 2009.

[2] E.E. Adams and L.W. Gelhar. Field study of dispersion in a heterogeneous aquifer: 2. spatial moments analysis. *Water Resources Research*, 28(12):3293–3307, 1992.

[3] L. Afraites. A new coupled complex boundary method (ccbm) for an inverse obstacle problem. *Discrete & Continuous Dynamical Systems-Series S*, 15(1), 2022.

[4] M. Alosaimi and D. Lesnic. Determination of a space-dependent source in the thermal-wave model of bio-heat transfer. *Computers & Mathematics with Applications*, 129:34–49, 2023.

[5] H. Ammari, E. Bretin, J. Garnier, W. Jing, H. Kang, and A. Wahab. Localization, stability, and resolution of topological derivative based imaging functionals in elasticity. *SIAM Journal on Imaging Sciences*, 6(4):2174–2212, 2013.

[6] H. Ammari, J. Garnier, W. Jing, H. Kang, M. Lim, K. Sølna, and H. Wang. *Mathematical and statistical methods for multistatic imaging*, volume 2098. Springer, Switzerland, 2013.

[7] H. Ammari, J. Garnier, V. Jugnon, and H. Kang. Stability and resolution analysis for a topological derivative based imaging functional. *SIAM Journal on Control and Optimization*, 50(1):48–76, 2012.

[8] H. Ammari and H. Kang. *Reconstruction of small inhomogeneities from boundary measurements*. Lectures Notes in Mathematics vol. 1846. Springer-Verlag, Berlin, 2004.

[9] S. Amstutz, I. Horchani, and M. Masmoudi. Crack detection by the topological gradient method. *Control and Cybernetics*, 34(1):81–101, 2005.

[10] M. Andrle and A. El Badia. Identification of multiple moving pollution sources in surface waters or atmospheric media with boundary observations. *Inverse Problems*, 28:075009, 2012.

[11] B. Berkowitz, J. Klafter, R. Metzler, and H. Scher. Physical pictures of transport in heterogeneous media: Advection-dispersion, random-walk, and fractional derivative formulations. *Water Resources Research*, 38(10):9–1, 2002.

[12] A. Canelas, A. Laurain, and A. A. Novotny. A new reconstruction method for the inverse potential problem. *Journal of Computational Physics*, 268:417–431, 2014.

[13] A. Canelas, A. Laurain, and A. A. Novotny. A new reconstruction method for the inverse source problem from partial boundary measurements. *Inverse Problems*, 31(7):075009, 2015.

[14] B.A. Carreras, V.E. Lynch, and G.M. Zaslavsky. Anomalous diffusion and exit time distribution of particle tracers in plasma turbulence model. *Physics of Plasmas*, 8(12):5096–5103, 2001.

[15] F. Caubet, C. Conca, and M. Godoy. On the detection of several obstacles in 2D Stokes flow: Topological sensitivity and combination with shape derivatives. *Inverse Problems and Imaging*, 10(2):327–367, 2016.

[16] F. Caubet and M. Dambrine. Localization of small obstacles in stokes flow. *Inverse Problems*, 28(10):1–31, 2012.

[17] T. Chan and X. Tai. Level set and total variation regularization for elliptic inverse problems with discontinuous coefficients. *Journal of Computational Physics*, 193:40–66, 2003.

[18] A.V. Chechkin, V.Y. Gonchar, and M. Szydlowsky. Fractional kinetics for relaxation and superdiffusion in a magnetic field. *Physics of Plasmas*, 9(1):78–88, 2002.

[19] J. Cheng, J. Nakagawa, M. Yamamoto, and T. Yamazaki. Uniqueness in an inverse problem for a one-dimensional fractional diffusion equation. *Inverse Problems*, 25(11):115002, 2009.

[20] X. Cheng, R. Gong, W. Han, and X. Zheng. A novel coupled complex boundary method for solving inverse source problems. *Inverse Problems*, 30(5):055002, 2014.

[21] M. Dalla Riva, M.L. de Cristoforis, and P. Musolino. *Singularly perturbed boundary value problems: A functional analytic approach*. Springer Nature Switzerland, 2021.

[22] R. Dautray and J. L. Lions. *Mathematical analysis and numerical methods for science and technology. Volume 2 – Functional and Variational Methods*. Springer-Verlag, Berlin, Heidelberg, New York, 1988.

[23] L. Debnath. Recent applications of fractional calculus to science and engineering. *International Journal of Mathematics and Mathematical Sciences*, 2003(54):3413–3442, 2003.

[24] M. C. Delfour and J. P. Zolésio. *Shapes and Geometries. Advances in Design and Control*. Society for Industrial and Applied Mathematics (SIAM), Philadelphia, PA, 2001.

[25] A. El Badia and T. Ha-Duong. On an inverse problem for the heat equation. Application to a pollution detection problem. *Inverse Ill-Posed Problems*, 10(6):585–599, 2002.

[26] J. Ferchichi, M. Hassine, and H. Khenous. Detection of point-forces location using topological algorithm in stokes flows. *Applied Mathematics and Computation*, 219(12):7056–7074, 2013.

[27] K. Fujishiro and Y. Kian. Determination of time dependent factors of coefficients in fractional diffusion equations. *Mathematical Control & Related Fields*, 6(2):251–269, 2016.

[28] S. Garreau, Ph. Guillaume, and M. Masmoudi. The topological asymptotic for PDE systems: the elasticity case. *SIAM Journal on Control and Optimization*, 39(6):1756–1778, 2001.

[29] M. Giona, S. Cerbelli, and H.E. Roman. Fractional diffusion equation and relaxation in complex viscoelastic materials. *Physica A: Statistical Mechanics and its Applications*, 191(1-4):449–453, 1992.

[30] R. Gong, X. Cheng, and W. Han. A new coupled complex boundary method for bioluminescence tomography. *Communications in Computational Physics*, 19(1):226–250, 2016.

[31] R. Gong, X. Cheng, and W. Han. A coupled complex boundary method for an inverse conductivity problem with one measurement. *Applicable Analysis*, 96(5):869–885, 2017.

[32] R. Gorenflo, Y. Luchko, and M. Yamamoto. Time-fractional diffusion equation in the fractional sobolev spaces. *Fractional Calculus and Applied Analysis*, 18(3):799–820, 2015.

[33] A. Henrot and M. Pierre. *Variation et optimisation de formes: une analyse géométrique*, volume 48. Springer Science & Business Media, 2006.

[34] L. Hörmander. *The analysis of linear partial differential operators I. Distribution Theory and Fourier Analysis*. Springer-Verlag, Berlin, 2003.

[35] M. Hrizi, A.A. Novotny, and R. Prakash. Reconstruction of the source term in a time-fractional diffusion equation from partial domain measurement. *The Journal of Geometric Analysis*, 33(6):168, 2023.

[36] X. Hu and S. Zhu. On geometric inverse problems in time-fractional subdiffusion. *SIAM Journal on Scientific Computing*, 44(6):A3560–A3591, 2022.

[37] V. Isakov, S. Leung, and J. Qian. A fast local level set method for inverse gravimetry. *Communications in Computational Physics*, 10(4):1044–1070, 2011.

[38] A. Jeffrey and H.H. Dai. *Handbook of mathematical formulas and integrals*. Elsevier, 2008.

[39] D. Jiang, Z. Li, Y. Liu, and M. Yamamoto. Weak unique continuation property and a related inverse source problem for time-fractional diffusion-advection equations. *Inverse Problems*, 33(5):055013, 2017.

[40] D. Jiang, Z. Li, M. Pauron, and M. Yamamoto. Uniqueness for fractional nonsymmetric diffusion equations and an application to an inverse source problem. *Mathematical Methods in the Applied Sciences*, 46(2):2275–2287, 2023.

[41] D. Jiang, Y. Liu, and D. Wang. Numerical reconstruction of the spatial component in the source term of a time-fractional diffusion equation. *Advances in Computational Mathematics*, 46(:):1–24, 2020.

[42] B. Jin, Y. Kian, and Z. Zhou. Reconstruction of a space-time-dependent source in subdiffusion models via a perturbation approach. *SIAM Journal on Mathematical Analysis*, 53(4):4445–4473, 2021.

[43] B. Jin, R. Lazarov, J. Pasciak, and Z. Zhou. Error analysis of semidiscrete finite element methods for inhomogeneous time-fractional diffusion. *IMA Journal of Numerical Analysis*, 35(2):561–582, 2015.

[44] B. Jin, R. Lazarov, and Z. Zhou. Error estimates for a semidiscrete finite element method for fractional order parabolic equations. *SIAM Journal on Numerical Analysis*, 51(1):445–466, 2013.

[45] B. Jin and W. Rundell. A tutorial on inverse problems for anomalous diffusion processes. *Inverse Problems*, 31(3):035003, 2015.

[46] G.K. Kalisch. A functional analysis proof of titchmarsh's theorem on convolution. *Journal of Mathematical Analysis and Applications*, 5(2):176–183, 1962.

[47] J. Kemppainen and K. Ruotsalainen. Boundary integral solution of the time-fractional diffusion equation. *Integral Equations and Operator Theory*, 64:239–249, 2009.

[48] Y. Kian, E. Soccorsi, Q. Xue, and M. Yamamoto. Identification of time-varying source term in time-fractional diffusion equations. *Communications in Mathematical Sciences*, 20(1):53–84, 2022.

[49] Y. Kian and M. Yamamoto. Reconstruction and stable recovery of source terms and coefficients appearing in diffusion equations. *Inverse Problems*, 35(11):115006, 2019.

[50] Y. Kian and M. Yamamoto. Well-posedness for weak and strong solutions of non-homogeneous initial boundary value problems for fractional diffusion equations. *Fractional Calculus and Applied Analysis*, 24:168–201, 2021.

[51] A.A. Kilbas, H.M Srivastava, and J.J. Trujillo. *Theory and applications of fractional differential equations*, volume 204. Elsevier, 2006.

[52] A. Kubica, K. Ryszewska, and M. Yamamoto. *Time-fractional Differential Equations: A Theoretical Introduction*. Springer Japan, ToKyo, 2020.

[53] B. Li and X. Xie. Regularity of solutions to time fractional diffusion equations. *Discrete and Continuous Dynamical Systems-B*, 24(7):3195–3210, 2019.

[54] X. Li and C. Xu. A space-time spectral method for the time fractional diffusion equation. *SIAM Journal on Numerical Analysis*, 47(3):2108–2131, 2009.

[55] Z. Li and Z. Zhang. Unique determination of fractional order and source term in a fractional diffusion equation from sparse boundary data. *Inverse Problems*, 36(11):115013, 2020.

[56] J. L. Lions and E. Magenes. *Problèmes aux limites non homogènes et applications*, volume 1,2. Dunod, Paris, 1968.

[57] F. Liu, P. Zhuang, V. Anh, I. Turner, and K. Burrage. Stability and convergence of the difference methods for the space–time fractional advection–diffusion equation. *Applied Mathematics and Computation*, 191(1):12–20, 2007.

[58] J.J. Liu and M. Yamamoto. A backward problem for the time-fractional diffusion equation. *Applicable Analysis*, 89(11):1769–1788, 2010.
[59] Y. Liu, Z. Li, and M. Yamamoto. Inverse problems of determining sources of the fractional partial differential equations. *Handbook of Fractional Calculus with Applications*, 2:411–430, 2019.
[60] M.M. Meerschaert and C. Tadjeran. Finite difference approximations for fractional advection-dispersion flow equations. *Journal of Computational and Applied Mathematics*, 172(1):65–77, 2004.
[61] P. Menoret, M. Hrizi, and A.A. Novotny. On the Kohn–Vogelius formulation for solving an inverse source problem. *Inverse Problems in Science and Engineering*, 29(1):56–72, 2021.
[62] R. Metzler and J. Klafter. Boundary value problems for fractional diffusion equations. *Physica A: Statistical Mechanics and its Applications*, 278(1–2):107–125, 2000.
[63] R. Metzler and J. Klafter. The random walk's guide to anomalous diffusion: a fractional dynamics approach. *Physics Reports*, 339(1):1–77, 2000.
[64] A. A. Novotny and J. Sokołowski. *Topological derivatives in shape optimization*. Interaction of Mechanics and Mathematics. Springer-Verlag, Berlin, Heidelberg, 2013.
[65] R. Prakash, M. Hrizi, and A.A. Novotny. A noniterative reconstruction method for solving a time-fractional inverse source problem from partial boundary measurements. *Inverse Problems*, 38(1):015002, 2022.
[66] J.F.T. Rabago. On the new coupled complex boundary method in shape optimization framework for solving stationary free boundary problems. *Mathematical Control and Related Fields*, pages pp–37, 2022.
[67] J.F.T. Rabago, L. Afraites, and H. Notsu. Detecting an immersed obstacle in stokes fluid flow using the coupled complex boundary method. *SIAM Journal on Control and Optimization*, 63(2):822–851, 2025.
[68] W. Rundell and Z. Zhang. Recovering an unknown source in a fractional diffusion problem. *Journal of Computational Physics*, 368:299 – 314, 2018.
[69] K. Sakamoto and M. Yamamoto. Initial value/boundary value problems for fractional diffusion-wave equations and applications to some inverse problems. *Journal of Mathematical Analysis and Applications*, 382(1):426–447, 2011.
[70] K. Sakamoto and M. Yamamoto. Inverse source problem with a final overdetermination for a fractional diffusion equation. *Mathematical Control & Related Fields*, 1(4):509, 2011.
[71] J. Sokołowski and A. Żochowski. On the topological derivative in shape optimization. *SIAM Journal on Control and Optimization*, 37(4):1251–1272, 1999.
[72] V.E. Tarasov. *Fractional dynamics: applications of fractional calculus to dynamics of particles, fields and media*. Nonlinear Physical Science, Springer, Berlin Heidelberg, 2011.
[73] E.C. Titchmarsh. The zeros of certain integral functions. *Proceedings of the London Mathematical Society*, 2(1):283–302, 1926.
[74] G. Wang, Y. Li, and M. Jiang. Uniqueness theorems in bioluminescence tomography. *Medical Physics*, 31(8):2289–2299, 2004.
[75] J.G. Wang, Y.B. Zhou, and T. Wei. Two regularization methods to identify a space-dependent source for the time-fractional diffusion equation. *Applied Numerical Mathematics*, 68:39–57, 2013.
[76] T. Wei, X.L. Li, and Y.S. Li. An inverse time-dependent source problem for a time-fractional diffusion equation. *Inverse Problems*, 32(8):085003, 2016.
[77] T. Wei and J. Wang. A modified quasi-boundary value method for an inverse source problem of the time-fractional diffusion equation. *Applied Numerical Mathematics*, 78:95–111, 2014.
[78] T. Wei and J.G. Wang. A modified quasi-boundary value method for the backward time-fractional diffusion problem. *ESAIM: Mathematical Modelling and Numerical Analysis*, 48(2):603–621, 2014.
[79] M. Yamamoto. Weak solutions to non-homogeneous boundary value problems for time-fractional diffusion equations. *Journal of Mathematical Analysis and Applications*, 460(1):365–381, 2018.
[80] M. Yamamoto. Fractional calculus and time-fractional differential equations: revisit and construction of a theory. *Mathematics*, 10(5):698, 2022.
[81] Y. Zhang and X. Xu. Inverse source problem for a fractional diffusion equation. *Inverse Problems*, 27(3):035010, 2011.
[82] X. Zheng, X. Cheng, and R. Gong. A coupled complex boundary method for parameter identification in elliptic problems. *International Journal of Computer Mathematics*, 97(5):998–1015, 2020.

(Mourad Hrizi) Monastir University, Department of Mathematics, Faculty of Sciences, Avenue de l'Environnement 5000, Monastir, Tunisia
*Email address*: mourad-hrizi@hotmail.fr

(Ravi Prakash) Departamento de Matemática, Facultad de Ciencias Físicas y Matemáticas, Universidad de Concepción, Avenida Esteban Iturra s/n, Bairro Universitario, Casilla 160 C, Concepción, Chile.
*Email address*: rprakash@udec.cl

(Antonio André Novotny) Laboratório Nacional de Computação Científica LNCC/MCTI, Coordenação de Métodos Matemáticos e Computacionais, Av. Getúlio Vargas 333, 25651-075 Petrópolis - RJ, Brasil
*Email address*: novotny@lncc.br